Applied Thermal Engineering xxx (2016) xxx–xxx

Contents lists available at ScienceDirect

Applied Thermal Engineering

journal homepage: www.elsevier.com/locate/apthermeng

Research Paper

Flow boiling in microchannels: Fundamentals and applications

T.G. Karayiannis [a,*], M.M. Mahmoud [a,b]

[a] Brunel University London, Kingston Lane, Uxbridge, Middlesex UB8 3PH, UK
[b] Zagazig University, Zagazig 44519, Egypt

HIGHLIGHTS

- Flow boiling is a promising method of transferring high heat fluxes.
- Flow boiling in microchannel heat sinks has wide applications in high heat flux devices.
- Fundamental thermofluid phenomena in microchannels are presented.
- Correlations are provided to predict flow pattern transition boundaries for small to micro tubes.
- Correlations giving the heat transfer coefficient for the design of microchannels are provided.

ARTICLE INFO

Article history:
Received 25 March 2016
Revised 15 July 2016
Accepted 10 August 2016
Available online xxxx

Keywords:
Flow boiling
Heat transfer
Critical heat flux
Single small to microtubes
Rectangular microchannels

ABSTRACT

The rapid advances in performance and miniaturization of electronics and high power devices resulted in huge heat flux values that need to be dissipated effectively. The average heat flux in computer chips is expected to reach 2–4.5 MW/m^2 with local hot spots 12–45 MW/m^2 while in IGBT modules, the heat flux at the chip level can reach 6.5–50 MW/m^2. Flow boiling in microchannels is one of the most promising cooling methods for these and similar devices due to the capability of achieving very high heat transfer rates with small variations in the surface temperature. However, several fundamental issues are still not understood and this hinders the transition from laboratory research to commercial applications. The present paper starts with a discussion of the possible applications of flow boiling in microchannels in order to highlight the challenges in the thermal management for each application. In this part, the different integrated systems using microchannels were also compared. The comparison demonstrated that miniature cooling systems with a liquid pump were found to be more efficient than miniature vapour compression refrigeration systems. The paper then presents experimental research on flow boiling in single tubes and rectangular multichannels to discuss the following fundamental issues: (1) the definition of microchannel, (2) flow patterns and heat transfer mechanisms, (3) flow instability and reversal and their effect on heat transfer rates, (4) effect of channel surface characteristics and (5) prediction of critical heat flux.

Areas where more research is needed were clearly mentioned. In addition, correlations for the prediction of the flow pattern transition boundaries and heat transfer coefficients in small to mini/micro diameter tubes were developed recently by the authors and presented in this paper.

1. Introduction

Microchannel heat exchangers have the potential of achieving very high heat transfer rates compared to conventional heat exchangers due to the very high surface area to volume ratio. For example, Kang et al. [1] tested the performance of a cross flow microchannel heat exchanger using de-ionized water. The core volume of this heat exchanger was 0.918 cm^3 (1 cm × 1 cm × 1 cm) and consisted of 26 stacked layers of silicon substrate with 125 channels etched on top of each layer resulting in a total surface area to volume ratio of 15,294 m^2/m^3. They reported that the heat transfer rate between the hot and cold fluid streams reached 5 kW at 4.5 l/min liquid flow rate, 2.47 bar pressure drop and 30 K mean temperature difference. In other words, this micro heat exchanger achieved a volumetric heat transfer rate of 5.44 GW/m^3 at about 24 W pumping power. This value is huge compared to existing compact heat exchangers. For instance, using the specifications published by a typical heat exchanger manufacturer, one can see

* Corresponding author.
E-mail addresses: tassos.karayiannis@brunel.ac.uk (T.G. Karayiannis), mbasuny@zu.edu.eg, mohamed.mahmoud@brunel.ac.uk (M.M. Mahmoud).

http://dx.doi.org/10.1016/j.applthermaleng.2016.08.063
1359-4311/

Nomenclature

Bd	Bond number (-), $g\Delta\rho D^2/\sigma$
Bo	Boiling number (-), q/Gh_{fg}
Co	confinement number (-), $\sqrt{\sigma/g\Delta\rho}/D$
D	diameter (m)
D_{th}	threshold diameter (m)
Eo	Eotvos number (-), $g\Delta\rho D^2/\sigma$
f_l	Fanning friction factor (-)
Fr_{gs}	Froude number (-), $Fr_{gs} = u_{gs}/\sqrt{gD}$
Fr^*_{gs}	modified Froude number $Fr^*_{gs} = u_{gs}\sqrt{\rho_g/\Delta\rho gD}$
F_{New}	new convective boiling enhancement factor (-)
g	acceleration of gravity (m/s^2)
G	mass flux (kg/m^2 s)
h_{sub}	enthalpy of inlet subcooling (J/kg)
h_{fg}	latent heat (J/kg)
k_f	liquid thermal conductivity (W/m K)
L	length (m)
La	Laplace constant (-), $\sqrt{\sigma/g\Delta\rho}$
N_{co}	convection number (-), $((1-x)/x)^{0.8}(\rho_L/\rho_g)^{0.5}$
P	pressure (Pa)
$\Delta P_{restrictor}$	pressure loss across inlet restrictor (Pa)
q	heat flux (W/m^2)
Re_{Lo}	liquid only Reynolds number (-), GD/μ
Re_f	liquid Reynolds number (-), $(1-x)GD/\mu_f$
Re_{ls}	Reynolds number defined based on the liquid superficial velocity (-)
Re_{gs}	Reynolds number defined based on the gas superficial velocity (-)
U_r	relative velocity (m/s)
U_{ch}	channel velocity
u_{gs}	gas superficial velocity (m/s)
u_{ls}	liquid superficial velocity (m/s)
u_h	homogeneous velocity (m/s)
S_{New}	new nucleate boiling suppression factor (-)
We	Weber number, $G^2D/\sigma\rho_f$
We_L	Weber number based on the channel length, $G^2L/\sigma\rho_f$
We_r	Weber number based on the relative velocity, $\rho U_r^2 D/\sigma$
We_{gs}	Weber number based on the gas superficial velocity, $\rho u_{gs}^2 D/\sigma$
We_{ls}	Weber number based on the liquid superficial velocity, $\rho u_{ls}^2 D/\sigma$
x	vapour quality (-)
x_{in}	inlet vapour quality (-)
x_{crit}	critical vapour quality (-)

Greek symbols

α_c	critical void fraction (-)
α_{tp}	two phase heat transfer coefficient (W/m^2 K)
β	surface area density (m^2/m^3)
μ_g	gas viscosity (Pa s)
μ_l	liquid viscosity (Pa s)
$\Delta\rho$	difference between liquid and gas density (kg/m^3)
ΔT_{sub}	inlet sub-cooling (K)
Θ	contact angle (°)
ρ_L	liquid density (kg/m^3)
ρ_g	gas density (kg/m^3)
σ	surface tension (N/m)

that a compact heat exchanger of 12 kW has overall dimensions of 1630 cm^3, weights approximately 3 kg, has a surface area to volume ratio of 650 m^2/m^3 and a volumetric heat transfer rate of approximately only 14 MW/m^3. This example demonstrates that the surface area to volume ratio and the heat transfer rate per unit volume of microchannel heat exchangers are significantly higher than that of typical compact heat exchangers. Accordingly, microchannel heat exchangers are very useful means for process intensification, recovery of low grade waste energy and improving overall system performance. Based on that, more research was directed in the last two decades towards investigating flow boiling in microchannel heat exchangers with the objective of cooling high heat flux systems such as electronic equipment, laser diodes, insulated gate bipolar transistors (IGBTs) and fuel cells. The significant advantages of using flow boiling in these systems can be summarized as follows: (1) Flow boiling can achieve small variations in the surface temperature (almost uniform at values slightly above the saturation temperature). This can improve the durability of the electronic equipment significantly due to the reduction of the thermo-mechanical stresses inside the chip. Chamund et al. [2] reported that thermo-mechanical stresses are the main reason of failure in IGBT inverters used in traction applications. Single phase liquid cooling can also achieve small temperature variations in the chip. However, this requires very high liquid flow rates (turbulent flow), which requires a large pump and thus the overall cooling system will be bulky (see also point 2 that follows). (2) The capability of achieving very high heat transfer rates at small liquid flow rates compared to single phase cooling. This means that a small liquid pump is required resulting in a very compact cooling system. (3) If nucleate boiling is assumed, as claimed by some numbers of the research community, to be the dominant heat transfer mechanism in microchannels, another two advantages may be added. The first one is the increase of the heat transfer coefficient with increasing heat flux in nucleate boiling. This will result in very small variations in the chip temperature when the heat dissipation rate varies (increase/decrease). For example, for flow boiling of R-134a in a 1 mm diameter tube when the heat flux was increased from 13 kW/m^2 to 25 kW/m^2, the heat transfer coefficient increased from 6000 W/m^2 K to 8000 W/m^2 K, see Mahmoud et al. [3]. Based on these values at 8 bar system pressure (T_{sat} = 31.3 °C), the surface temperature increases only by 3% for this 12 kW/m^2 increase in heat flux. In contrast, if single phase liquid cooling was used, the surface temperature increases by about 60%. The significant variations in chip temperature in single phase flow when the heat dissipation rate varies may affect the lifetime of the electronic equipment. Nnanna et al. [4] mentioned that the failure rate of electronic components increases by a factor of two for every 10 K rise in temperature. The second advantage of nucleate boiling is the independence of the heat transfer coefficient on mass flux. This makes it possible to use a fixed speed pump, i.e. no need for a speed controller, which will result in a simpler and more reliable cooling system at a reduced cost.

Despite the advantages of flow boiling microchannel heat sinks, several fundamental issues are still not understood. These issues include the following: (1) The lack of a generally accepted definition for what is called "small/mini/microchannel". (2) The difficulty in triggering boiling, i.e. very high wall superheat is required at boiling incipience, see Yen et al. [5]. (3) The wall superheat increases significantly with increasing heat flux in some experimental conditions. For example, in a study by Koşar et al. [6], for water flow boiling in silicon microchannels, the wall superheat reached a value of about 80 K at the highest heat flux in their study (surface temperature 180 °C at 6.7 MW/m^2). Both the above issues require a great deal of work on enhancing the inner surface

Please cite this article in press as: T.G. Karayiannis, M.M. Mahmoud, Flow boiling in microchannels: Fundamentals and applications, Appl. Therm. Eng. (2016), http://dx.doi.org/10.1016/j.applthermaleng.2016.08.063

structure of the microchannel in order to reduce the wall superheat. (4) The lack of a generally accepted prediction methods for flow patterns, heat transfer and pressure drop. (5) Early dryout (low critical heat flux) and the unclear understanding of its dependence on the operating parameters. (6) Flow reversal and instabilities. (7) Unclear heat transfer mechanism(s). The present paper discusses some of these fundamental issues in separate sections. The paper starts with some possible applications of microchannel heat exchangers in order to understand the challenges in each application.

2. Applications of microchannel heat sinks

Mudawar [7] presented a detailed discussion on the possible applications of microchannel heat sinks including straight, serpentine and curved channels. The discussion below is only for heat sinks with straight parallel channels, which is very relevant to applications that have a planar geometry. These applications include cooling components in computers and information technology (CPUs, GPUs, memory cards, data storage devices), cooling high power semiconductor devices (IGBT inverters and switch-mode power supplies), cooling laser diode arrays, cooling proton exchange membrane fuel cells and evaporators/condensers in miniature vapour compression refrigerators. Some of these applications are discussed below.

2.1. Computer and IT industry

The International Technology Roadmap of Semiconductors (ITRS 2011) predicted that the power dissipation from a microprocessor chip will exceed 800 W by 2026 (the predicted value for 2015 was about 270 W). The value reached 240 W for ORACLE SPARC T4 processor produced by Oracle Corporation in 2011 for high performance computers. This processor has a typical die size value of 403 mm^2 resulting in a heat flux value of about 0.6 MW/m^2. For desktop computers, the die size is smaller than that in high performance computers. For example, Intel core i7-4790K processor produced by Intel in 2014 has a die size value of 177 mm^2 and dissipates 88 W. Accordingly, the average heat flux could reach values of 2 MW/m^2 in high performance computers and 4.5 MW/m^2 in desktop computers by 2026. Additionally, local hot spots (huge local heat fluxes) are very common in electronics chips. A few years ago, Bachmann and Bar-Cohen [8] reported that the hot spots can be 6–10 times the chip average power. Based on that, the hot spots could be as high as 27–45 MW/m^2 by 2026 in desktop computers and 12–20 MW/m^2 in high performance computers. It is worth mentioning that the higher the chip temperature, the lower the performance. Yang et al. [9] stated that the processor speed decreases by 10–15% as a result of the local hot spots (high local temperature). All heat flux values mentioned above are based on the abovementioned die sizes. It is important to note that, the chip temperature should be kept below 85 °C.

The huge heat flux values mentioned above cannot be met using existing cooling techniques. Tullius et al. [10] reported that the air cooling technique cannot dissipate more than 1 MW/m^2. Also, earlier, Jiang et al. [11] stated that conventional heat pipes cannot dissipate more than few tens of watts due to limitations in the wick thickness and cross sectional area of the pipe. Even with advanced heat pipes, such as pulsating and loop heat pipes, the maximum attainable heat flux is still very low. For instance, Qu et al. [12] designed and tested a silicon-based micro pulsating heat pipe consisting of trapezoidal microchannels with 0.352 mm hydraulic diameter using FC-72 and R-113 as the test fluids. The results demonstrated that with FC-72 the critical heat flux was 0.11 MW/m^2 while it was 0.086 MW/m^2 for R-113. Recently, Wan et al. [13] developed and tested a new design for a miniature loop heat pipe, which was filled with water-copper nano fluid. The new design included segregating the liquid and vapour flow passages and using a flat evaporator section consisting of parallel channels with enhanced surface. With this design, a maximum heat flux of 0.125 MW/m^2 was attained. Some researchers investigated cooling by liquid jet impingement, which was reported to dissipate high heat flux values. For example, Fabbri and Dhir [14] reported 3.1 MW/m^2 using fluid FC-40, Mudawar et al. [15] reported 1.5–2 MW/m^2 using fluid HFE-7100, Bostanci et al. [16] reported 4 MW/m^2 using anti-freeze coolant and Zhao et al. [17] reported 6.74 MW/m^2 using water impingement over a porous structure. Although this technique seems promising, Silk et al. [18] reported that the integration of spray cooling into a closed loop system configuration is still challenging. Additionally, it requires high pumping power and there is a danger of surface erosion. Single and two phase flow in microchannels can dissipate high heat flux values. Single phase water flow in silicon microchannel heat sinks was studied by Tuckerman and Pease [19] in a paper that stimulated a lot of follow up research for cooling very large scale integrated circuits. This heat sink dissipated a heat flux of 7.9 MW/m^2 at a surface temperature of 94 °C and a pressure drop of 2.04 bar. Escher et al. [20] tested a manifold microchannel heat sink and reported more than 7 MW/m^2 at 0.22 bar pressure drop using water as the test fluid. This design achieved about ten times reduction in pressure drop compared to the value measured by Tuckerman and Pease [19]. This may be suitable for short lengths electronic devices. However, in longer heated surfaces, pressure drop and temperature gradient may still be a problem. In flow boiling, Kandlikar et al. [21], for example, tested water in what they called "open channels with tapered manifold" made of copper and reported a heat flux of 5.06 MW/m^2 at a surface temperature of 125 °C and 0.22 bar pressure drop.

It is obvious that single and two phase flow in microchannels can achieve high heat flux. One of the important merits of on-chip cooling using single or two phase flow in microchannel heat sinks could be the possibility of low grade energy recovery in supercomputers and data centres. It is worth mentioning that the cooling load in computers is low, i.e. few hundreds of watts in a high performance personal computer accommodating one CPU and one GPU but it can be as high as thousands of kilowatts in supercomputers and data centres. For example, a super computer developed by the National Supercomputer Centre in Guangzhou, China ranked in the top 10, accommodates 3,120,000 processor cores and consumes (dissipates) about 17.81 MW (www.top500.org). The currently adopted chilled air cooling technique is not effective for energy recovery and consumes about 50% of the total power consumption by all IT equipment. Berkeley and Mahdavi [22] used a water cooled server produced by IBM and conducted a comparison study between air cooling and on-chip water cooling for a small supercomputer rated as 300 kW. The results demonstrated that the air cooling system consumed 44% of the rated power (0.44 × 300 kW) while the water cooling system consumed only 16.7% (0.167 × 300 kW) with 15% improvement in the overall energy efficiency. The water cooled IBM server (iDataplex 360) used in the above evaluation study is shown in Fig. 1. Marcinichen et al. [23] conducted a theoretical and experimental evaluation study for single phase water cooling, two phase pumped loop cooling system and vapour compression refrigeration cycle (VCC) using microchannel evaporators for applications in data centres. The theoretical evaluation study was conducted for a server with a total power of 3.7 kW. It was found that with single phase water cooling, the pumping power was 35 W, which was 5.5 times higher than that of the two phase pumped loop cooling system using R-134a and R-1234ze (6.4 W for R-134a and 7.9 W for R-1234ze). Additionally, the power consumption by the VCC was much higher,

Please cite this article in press as: T.G. Karayiannis, M.M. Mahmoud, Flow boiling in microchannels: Fundamentals and applications, Appl. Therm. Eng. (2016), http://dx.doi.org/10.1016/j.applthermaleng.2016.08.063

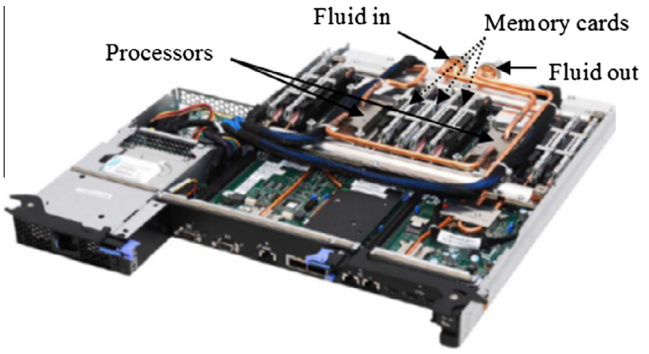

Fig. 1. Liquid cooled IBM iDataplex 360 Server, Berkeley and Mahdavi [22].

i.e. 95–117 times higher (746.5 W). Therefore, more energy savings are expected if boiling microchannel heat sinks were used, rather than single phase liquid cooling and a pump loop cooling system may be more efficient than a VCC system.

2.2. Miniature refrigeration systems

Small scale and miniature vapour compression refrigeration systems can be used in, for example, (i) portable units for cooling persons in harsh environments and (ii) cooling electronics devices. Microchannel evaporators and condensers are vital components of these miniature systems. A brief review is given in this section on the performance of these small systems as well as the advantages of incorporating micro heat exchangers in refrigeration and air conditioning systems. Using microchannel evaporators/condensers in small scale refrigeration systems can help reduce refrigerant charge and thus global warming and ozone layer depletion. For example, Pettersen et al. [24] reported that the annual emission of refrigerants is likely to exceed 100,000 tonnes, which corresponds to the impact of more than 150 million tonnes of CO_2. This figure is expected to decrease if microchannel heat exchangers are used wherever possible due to the significant reduction in refrigerant charge. In the vapour compression systems for high heat flux loads, the design has to consider not only the evaporator but also the condenser. Hrnjak and Litch [25] carried out an experimental study on a prototype ammonia chiller with an air-cooled condenser and flat tube evaporator. They tested two aluminium air-cooled condensers, one was a single serpentine macro-tube condenser (D = 4.06 mm) and the second was a parallel microchannels condenser (D_h = 0.7 mm). They reported that microchannels condensers reduced the specific charge by 76% (18 g/kW) compared to the serpentine macro-tube condenser. Additionally, the overall heat transfer coefficient in the microchannels condenser was 60–80% higher than that of the serpentine one.

A miniature vapour compression system consists of five main components, namely, a miniature compressor, a microchannel condenser, a throttling device, a microchannel evaporator and an accumulator. The performance of this system is assessed using the coefficient of performance (COP) defined as the ratio of the heat transfer rate at the evaporator to the input work to the compressor. Mongia et al. [26] tested a prototype miniature refrigeration system designed for cooling laptops. Two microchannel evaporators connected in series with cooling capacity of 40 and 10 W were included in the system. The expansion device was a capillary tube, 0.4 mm in inner diameter and 1.1 m in length. The miniature compressor was a positive displacement type driven by a 12 V DC power supply. It had a pressure ratio of 2.3. This compressor required external cooling using a fan such that its temperature was kept below 70 °C. The overall size of the system was small so that it can fit in a laptop form factor. The results demonstrated that a COP value greater than 2.25 can be achieved with this system. It is obvious that at this COP, the power consumption by the compressor is 22.2 W, which is about 44% of the total cooling load. The COP value is expected to be lower if the power consumption by the compressor cooling fan was included in the calculation of the COP. Wu et al. [27] designed and manufactured a micro compressor for a cooling capacity of 300 W. The compressor was made of high-Si aluminium alloy and was 50 mm in diameter, 70 mm in height, 400 g in weight and was driven by a brushless motor. The overall size of the system was 260 × 250 × 120 mm with a total weight of 2.85 kg. It was shown that with the 300 W cooling capacity, the COP was 2.3. In other words, the compressor consumed 130.4 W, which is again 43.5% of the cooling load. Accordingly, the authors concluded the need for compressors of higher efficiency.

Wu and Du [28] tested a miniature vapour compression refrigeration system with 200 W cooling load. A commercially available compressor, 58 mm in diameter and 78 mm in height and driven by 24 V DC power supply, was used. The overall size of the system was 300 × 230 × 70 mm and the weight was 3.49 kg. The expansion device was a capillary tube 0.8 mm in diameter and 1.8 m in length. The results demonstrated that the system performance depends on the refrigerant charge and the compressor speed and the optimum values were respectively 100 g and 2858 rpm. Additionally, the COP of the system varied from 2.7 to 3.4, which is higher than that reported by Mongia et al. [26] and Wu et al. [27]. Based on these values, the power consumption by the compressor varies from 58.8 to 74 W. Wu and Du [28] stated that system efficiency can be improved if the compressor losses are reduced and reported that more research is required to design more efficient compressors. The slight improvement in performance compared to the studies of Mongia et al. [26] and Wu et al. [27] could be attributed to the fact that Wu and Du [28] first optimized the system parameters (refrigerant charge, compressor speed and capillary tube) through conducting a set of experiments. Jeng and Teng [29] developed a hybrid cooling system that combines single phase liquid cooling and vapour compression refrigeration cooling. The single phase pumped loop system used an aluminium oxide-water nano fluid while the vapour compression refrigeration system used R290/R600a refrigerant. The system included a hybrid evaporator that had separate flow passages for the single phase liquid and the refrigerant such that the two systems could run at the same time. In the refrigeration system, a commercially available variable frequency DC rotary compressor (60 mm in diameter and 100 mm in height) was used, while a micro pump was used in the single phase pumped loop system. The overall size of this hybrid cooling system was 160 × 350 × 12 mm. The results demonstrated that the maximum cooling capacity achieved with the single phase pumped loop system was 450 W at 6.43 W pumping power while it was 270 W at 28 W compressor power consumption in the vapour compression system. Surprisingly, the results of the refrigeration cycle give a COP value of 9.6, which is very high compared to the studies discussed above. Also, it is obvious that the miniature pumped loop cooling system is more effective than the miniature vapour compression system. Combining the two systems together in a hybrid system resulted in a maximum cooling capacity of 540 W and total power consumption of 29.5 W. Yuan et al. [30] developed and tested a miniature portable vapour compression refrigerator for personal cooling applications. The system has overall dimensions 190 × 190 × 100 mm and weight 2.75 kg and consisted of a miniature compressor, a miniature electronic expansion valve, microchannel evaporator (0.35 × 0.35 mm^2 channel cross sectional area) and condenser (0.55 × 0.7 mm^2 channel cross sectional area). The experiments demonstrated that the system operated smoothly and reliably for a maximum cooling load of 260 W at 50 °C ambient

Please cite this article in press as: T.G. Karayiannis, M.M. Mahmoud, Flow boiling in microchannels: Fundamentals and applications, Appl. Therm. Eng. (2016), http://dx.doi.org/10.1016/j.applthermaleng.2016.08.063

temperature. The system was powered by a lithium battery. It is clear that the COP is very low compared to the above studies, i.e. the compressor consumes 160.5 W at a 260 W cooling load giving a COP value of 1.62.

The above studies focused mostly on the performance of the miniature cooling system without reporting on the reliability of the compressor. Truttasanawin et al. [31] tested the performance of a small-scale compressor in a miniature scale refrigeration system using R-134a. The compressor used in the system was a commercially available variable speed rotary compressor (8.5 cm in diameter and 16.6 cm in height) driven by a DC brushless motor. A manual needle valve was used as an expansion device. The results showed that the system was able to dissipate heat fluxes of approximately 40–75 W/cm^2 for a chip size of 1.9 cm^2. The COP of the system varied from 2.8 to 4.7 when the pressure ratio varied from 1.9 to 3.2. However, the compressor failed after 50 steady-state tests, which represented approximately 400 h of operation. They attributed this to the operation of the compressor outside its design operating range.

2.3. Cooling of IGBTs

Insulated gate bipolar transistors IGBTs are widely used in several applications such as electric vehicles, rail tractions, wind turbines, power supplies and motors. The maximum rated voltage and current of each IGBT module depends on the application and consequently the power dissipation varies significantly from one module to another. In order to understand the thermal management of IGBTs, a brief overview on the IGBT package is given in this section. Fig. 2a depicts a schematic drawing for an IGBT module package that accommodates one IGBT chip and one diode chip. The chips are attached to a direct-bonded copper (DBC) substrate (ceramic substrate sandwiched between copper layers) which is attached to a base plate using ceramic bonding. All the components of the package are housed in a plastic case and the heat sink is attached to the base plate using thermal grease. It is worth mentioning that an IGBT module can accommodate several IGBT and diode chips. An example of a typical IGBT module, which was produced by Mitsubishi Electric Corporation in 2015, is depicted in Fig. 2b. This module has the dimensions 150 × 166 mm^2, dissipates 6.52 kW and requires a maximum junction temperature of 175 °C (temperature at the chip-solder interface) and maximum case temperature value of 125 °C. In the catalogue of this module, the junction to case thermal resistance was 23 K/kW and 39 K/kW respectively for the IGBT and diode chips. Thus, for the maximum allowed temperature difference between the junction and the case (50 K), the power dissipated from the IGBT and the diode chip could be estimated as 2.17 kW and 1.28 kW respectively. According to the information published in www.abb.com, the die size of IGBT chips ranges from 6.5 × 6.6 mm^2 to 14.3 × 14.3 mm^2 and from 6.3 × 6.3 mm^2 to 14.3 × 14.3 mm^2 for the diode chips. If the average heat flux is calculated based on the overall size of the module, i.e. $q_{average}$ = 0.26 MW/m^2, a value that is very low, compared to the predicted average heat flux in computer chips. However, using the die sizes reported above and the estimated power dissipation rate from each chip, the heat flux at the chip base could be as high as 10–50 MW/m^2 for the IGBT chip and 6.3–30 MW/m^2 for the diode chip. These values are huge compared to the aforementioned average heat fluxes. Additionally, this example demonstrates that the heat fluxes in the IGBT chips are about two times higher than those in the diode chip. In other words, the local heat fluxes are not uniformly distributed inside the module - something that might result in severe temperature gradients in the substrate. Accordingly, an additional challenge in the thermal management of IGBT arises from the fact that the cooling system should take into account the non-uniform heat flux distribution inside the module. The operation at high temperatures and the temperature gradients inside the substrate result in significant thermal stresses inside the package. Owing to the difference in the coefficient of thermal expansion of the different materials inside the package, thermo-mechanical stresses were reported as the main reason of failure in IGBTs, Chamund et al. [2]. In addition to that, local hot spots are also very common in each chip. Fig. 3 taken from Wintrich et al. [32] depicts an infrared image of an IGBT chip having an active area of 12 × 12 mm^2. The temperature distribution is across the diagonal of the chip. The top part of the figure demonstrates that the hot spot is located nearly at the centre of the chip and the temperature difference between the edges and the centre of the chip was 41.8 K. The figure also shows the locations of the non-conducting gate area and bond wires, indicated by a drop in temperature. Cyclic operation with large temperature gradient inside the chip could result in chip failure if the heat was not dissipated effectively away from the chip. As previously mentioned in Section 1, two phase flow boiling in microchannels could be very efficient in cooling IGBT modules due to the capability of reducing the hot spots inside the chip. Saums [33] conducted an evaluation study for three cooling techniques used for cooling IGBT modules in electric vehicles. The three techniques were air cooling, single phase water cooling and two phase pumped loop cooling (fluid is circulated using a pump rather than a compressor) using R-134a refrigerant. It was found that using two phase cooling achieved the following over the other cooling methods: (1) much higher heat dissipation rates. The heat dissipation rate increased by 96% compared to water cooling and by 125% compared to air cooling

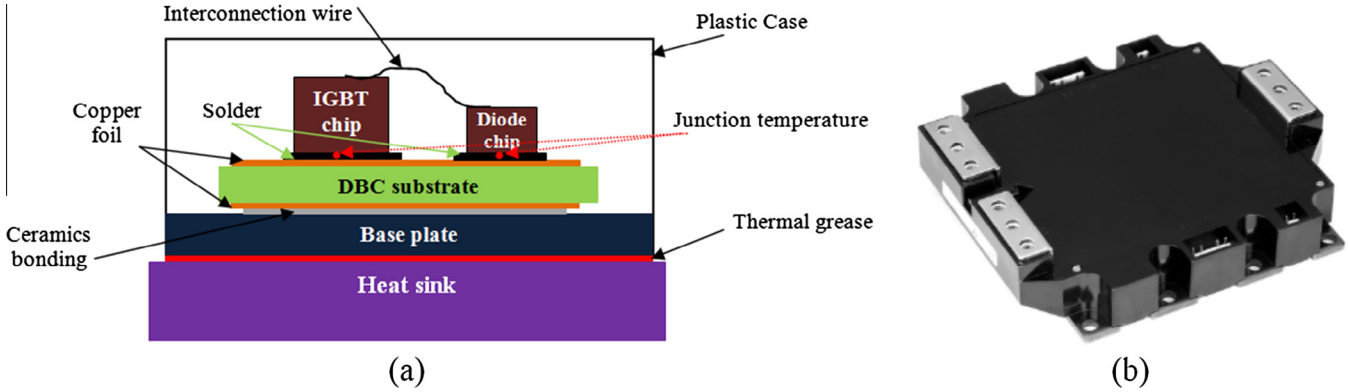

Fig. 2. (a) Schematic drawing for the components of IGBT module package and (b) CM900DUC-24S Mitsubishi IGBT module (DBC: direct-bonded copper), http://www.mitsubishielectric-mesh.com/products/pdf/CM900DUC-24S_N1.pdf.

Please cite this article in press as: T.G. Karayiannis, M.M. Mahmoud, Flow boiling in microchannels: Fundamentals and applications, Appl. Therm. Eng. (2016), http://dx.doi.org/10.1016/j.applthermaleng.2016.08.063

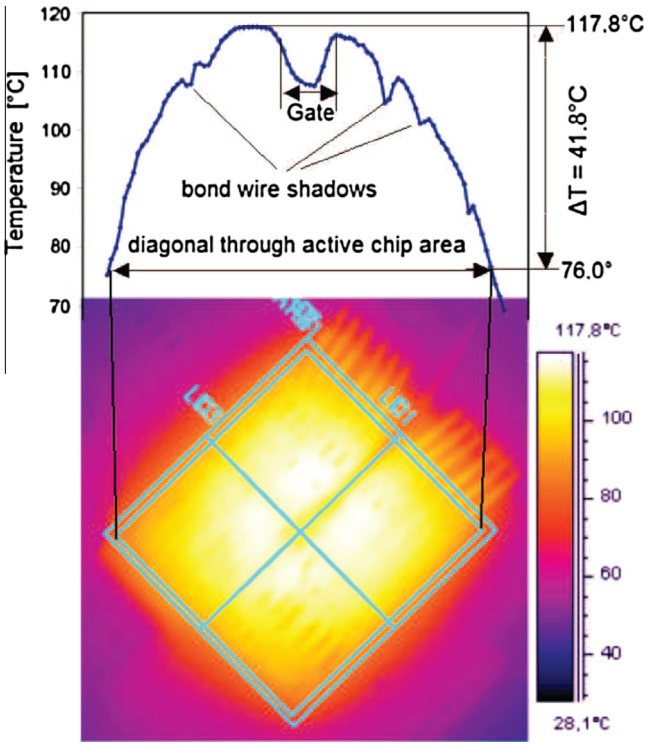

Fig. 3. Infrared image and the temperature distribution along the diagonal of an IGBT chip, Wintrich et al. [32].

and (2) significant reduction in size and weight. The size of the two phase pumped loop system decreased by 250% compared to the other cooling systems.

2.4. Cooling of PEM fuel cells

Fuel cells are energy conversion devices that convert chemical energy directly into electrical energy with no harmful emissions like fossil fuel combustion systems. The only by-product of a fuel cell is the generation of heat and water. Gao et al. [34] summarized the different types of fuel cells, among them the polymer electrolyte membrane fuel cell (PEMFC) and the direct methanol fuel cell (DMFC) in which the membrane is a solid polymer with an operating temperature of about 80 °C. The low operating temperature of this type of fuel cell means that the temperature difference between the coolant and the hot surface is small and consequently a huge heat transfer surface area is required in order to cool the cell and keep the operating temperature at about 80 °C. This can be achieved with microchannel heat exchangers. Fig. 4 depicts a schematic drawing of a fuel cell stack, consisting of two cells, to help explain the components and thermal management process of a fuel cell. A single cell consists of a fuel channels plate, oxidant channels plate, fuel diffusion layer, oxidant diffusion layer, fuel catalyst layer, oxidant catalyst layer and electrolyte membrane. In the case of liquid cooling, separate coolant channels are embedded between the cells as shown in the figure. The operating principle of a fuel cell is that the hydrogen-rich fuel is fed to the cathode through the channels plate then it passes through the fuel diffusion layer then a catalyst layer where the fuel is oxidized (release electrons and protons). The protons pass through the membrane and move towards the anode while the electrons flow into the external electric circuit. Pandiyan et al. [35] reported that the most important factors of heat dissipation in fuel cells are the irreversibility of the electrochemical reactions and joule heating. Additionally, Gao et al. [34] reported that the PEM fuel cells have a 50% conversion efficiency, high power density and have the advantage of quick start-up due to the low operating temperature, which makes them very suitable for portable and transportation applications. This efficiency means that the heat dissipation rate from a fuel cell is the same as the electric power generated by the cell, i.e. a fuel cell rated as 50 kW electric power can dissipate 50 kW of thermal energy. Also, Pandiyan et al. [35] reported that the heat dissipation rate depends on the cell operating voltage. At an operating voltage of 0.6 V, the heat dissipation rate was the same as the electric power produced by the cell. When the voltage decreased to 0.5 V, the heat dissipation rate was two times the electric power dissipation. This means that small variations in the operating voltage can result in significant changes to the heat dissipation rate, and thus the temperature distribution inside the stack. Pei et al. [36] measured the temperature distribution in the cathode plate of a PEM fuel cell stack using micro thermocouples embedded into the plate. The fuel cell stack consisted of 46 single cells with the following specifications: flow field channel cross section 0.75 × 1.5 mm, gas diffusion layer thickness 0.25 mm, PEM thickness 0.025 mm and catalyst layer thickness 0.012 mm. This stack was cooled using de-ionized water and four cells were selected for the measurements: The first, the last and two cells in the middle of the stack. It was found that the temperature distribution in the stack takes a parabolic shape, i.e. the temperature peaks at the cells located at the middle of the stack. The maximum temperature difference inside the stack was found to be 8 K.

Thermal management of fuel cell stacks is complex compared to electronics systems. In electronics, the target is to keep the chip temperature as low as possible for better performance. In contrast, the cooling system of fuel cells should keep the operating temperature uniform and as high as possible, but below the maximum operating temperature (80 °C). Barreras et al. [37] reported

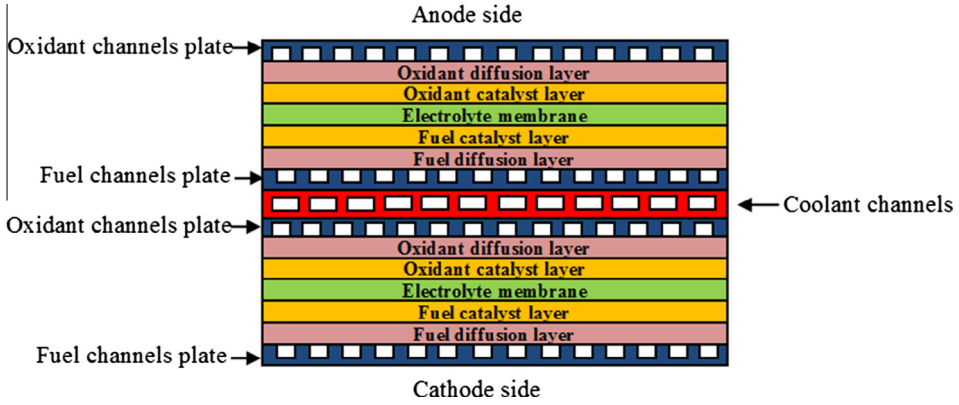

Fig. 4. Schematic drawing for the fuel cell stacks.

Please cite this article in press as: T.G. Karayiannis, M.M. Mahmoud, Flow boiling in microchannels: Fundamentals and applications, Appl. Therm. Eng. (2016), http://dx.doi.org/10.1016/j.applthermaleng.2016.08.063

that low cell temperatures may lead to water flooding in the electrolyte membrane. This prevents transport of the reactant gases, while high cell temperature may lead to dehydration of the membrane and consequently performance degradation. There is a very limited research on using flow boiling to cool fuel cells. Zhang and Kandlikar [38] conducted a review on the different methods adopted in cooling PEM fuel cells. The widely used methods were: (1) heat spreaders, such as high thermal conductivity materials and heat pipes, (2) air cooling, using separate air streams. It is worth mentioning that air cooling is not efficient for fuel cells exceeding 5 kW, as reported by Soupremanien et al. [39], and (3) single phase liquid cooling. They also highlighted the need for investigating two phase flow characteristics in parallel channels.

As mentioned above, there is limited research on two phase flow boiling in microchannels at the conditions that are relevant to fuel cell applications. Flow boiling, using a fluid such as HFE-7100, could be very efficient and suitable for the operating conditions of the low temperature fuel cells. The saturation temperature of this fluid at atmospheric pressure is 61 °C. Assuming wall superheat 12 K, the operating temperature of the stack could be maintained between 70 and 80 °C, which is the optimum operating temperature range for a PEM fuel cell. This could result in significant enhancements in performance, durability and system compactness.

The various possible applications of flow boiling in microchannels were presented above. In such applications, heat loads up to 2–4 MW/m^2 are already in some cases or will be typical soon with hot spots in, for example, computer chips expected to reach significantly higher values, e.g. 12–20 MW/m^2 in high performance computers and 27–45 MW/m^2 in desktop computers. In IGBT modules the heat flux values required can be as high 10–50 MW/m^2 for the IGBT chips and 6.3–30 MW/m^2 for diode chips. Since each module consists of a number of IGBT and diode chips with different heat fluxes, the heat flux is not uniformly distributed in the module. This requires an innovative cooling solution that accounts for the non-uniformity of heat flux distribution in each IGBT module. Flow boiling in microchannels can provide a very favourable cooling solution as it can cope more easily with non-uniform heat flux distribution in the substrate to be cooled.

A comparative assessment of thermal management systems such as pumped single phase, pumped two phase and vapour refrigeration systems indicate that the pumped two-phase system is the most efficient method for cooling high heat flux devices. More research is also needed in the design of small scale compressors if miniature vapour compressor systems are to be considered for such thermal management systems.

3. Definition of microchannel

One of the controversial issues in two phase flow is the lack of a precise definition for what is called "small/mini/microchannel". The accurate determination of the threshold between macro/small/mini/micro channels requires accurate experiments to be conducted in the same laboratory using a wide range of channel diameters with a high resolution (decreasing the diameter gradually in small steps). This process is difficult to achieve because it requires significant time and effort to cover all of the experimental conditions for each channel size. Thus, several researchers have investigated only a few channel sizes in order to get an insight into the onset of transition from the macro to the small/mini/micro scale. Accordingly, the word "micro" seems to be a general term used by researchers to refer to the channel size at which the macro scale two phase flow phenomena exhibit significant changes, i.e. the lower limit of macro scale phenomena. In other words, the term "micro scale" is a term that includes the three terms "small/mini/micro". Identifying the threshold between macro and micro (small/mini/microchannel) can help in segregating the experimental data in the literature and consequently the development of accurate correlations for micro scale applications. All previous attempts of researchers to differentiate between macro and micro scale can be divided into two groups. The first group proposed using fixed ranges of diameter or surface area per unit volume. Shah and Sekulić [40] used the surface area density (β) as a criterion to differentiate between macro, compact, meso and micro heat exchangers. Heat exchangers are regarded as compact if $\beta \geqslant 700\ m^2/m^3$, meso if $\beta \geqslant 3000\ m^2/m^3$ and micro if $\beta \geqslant 15{,}000\ m^2/m^3$. When these values of β are converted into hydraulic diameter, similar ranges to those given by Mehendale et al. [41] will result. These ranges are: $D > 6$ mm for macro exchangers, $D = 1$–6 mm for compact exchangers, $D = 0.1$–1 mm for meso exchangers and $D = 0.001$–0.1 mm for micro exchangers. Kandlikar and Grande [42] proposed different ranges based on the lower limit of channel manufacturing techniques for different heat exchangers applications. They have considered the exchangers as conventional when $D > 3$ mm, mini when $D = 0.2$–3 mm and micro when $D = 0.01$–0.2 mm.

The aforementioned classifications do not seem representative for two phase flows because they do not consider the physical mechanisms, different fluids or other flow effects. The absence of stratified flow in horizontal microchannels, and hence the fact that the orientation of the channel has no effect on two phase flow pattern, indicates the predominance of the surface tension force over gravity. Consequently, a second group of researchers have used surface tension force as a base to formulate a non-dimensional criterion for the transition from macro to micro scale. These include Eotvos number $E\ddot{o} = 4\pi^2$, recommended by Brauner and Moalem-Maron [43], confinement number $Co = 0.5$ by Cornwell and Kew [44], Bond number $Bd^{0.3} \leqslant 0.3$ by Suo and Griffith [45], Laplace constant $La = D$ by Triplett et al. [46] and $E\ddot{o} = 1.6$ by Ullmann and Brauner [47]. The definition of the above parameters is included in the nomenclature section. Ong and Thome [48] investigated flow patterns for R-134a, R-245fa and R-236fa in horizontal channels with diameter 1.03, 2.2, and 3.04 mm. They argued that there is no sudden transition from the macro to micro scale and the transition occurs gradually. Based on that they proposed $Co \approx 0.3$–0.4 for the transition from macro to meso scale and $Co = 1$ for the transition from meso to micro scale. The micro scale transition criterion is exactly the same as the one proposed by Triplett et al. [46] where $Co = 1$ is the same as $La = D$. Harirchian and Garimella [49] conducted a flow boiling study using FC-77 and microchannels with a wide range of cross sectional areas. They classified the flow regimes into confined and unconfined flows. The confined flow was considered as a feature of micro scale flow and they found that it depends on channel cross section and flow inertia. Accordingly, they proposed a macro to micro transition criterion based on what they called the "confinement-convective number", which equals to $Bd^{0.5} \times Re_{Lo} = 160$ (gravity, surface tension, inertia and viscous forces are considered). Tibirica and Ribatski [50] proposed two criteria for the transition from macro to micro scale flow. The first one was based on a mechanistic model for plug flow in a circular channel and the transition was assumed to occur when stratified flow no longer existed. In this model, a balance between the hydrostatic pressure and capillary forces was conducted and the transition was found to occur when $D = La\sqrt{8\cos\theta}$. Fig. 5

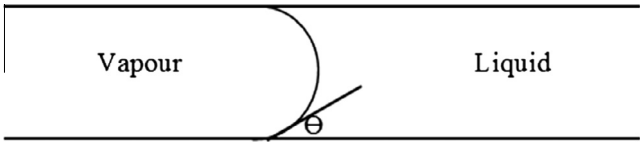

Fig. 5. Schematic drawing for the definition of the contact angle used in the model proposed by Tibirica and Ribatski [50].

Please cite this article in press as: T.G. Karayiannis, M.M. Mahmoud, Flow boiling in microchannels: Fundamentals and applications, Appl. Therm. Eng. (2016), http://dx.doi.org/10.1016/j.applthermaleng.2016.08.063

illustrates the definition of the angle Θ used in their model. They ignored the effects of inertia, which according to them was a reasonable assumption for the conditions of stratified flow. The second criterion was based on uniformity of the liquid film thickness in annular flow, which gave the transition occurring at $D = La\sqrt{1/20}$.

All the aforementioned criteria are summarized in Table 1. Each criterion was rewritten in a simple form to give the threshold diameter as a function of the Laplace constant $La = \sqrt{\sigma/g\Delta\rho}$. Also, the table compares the threshold diameters calculated for all criteria using water, three refrigerants and HFE-7100 at the same saturation temperature. The last column in the table shows the average value for the three refrigerants to establish a simple comparison with water. It is obvious from the table that there is no consensus on the threshold. However, the values predicted by the criterion given by Harirchian and Garimella [49] agree with those predicted by the second criterion (c2) given by Tibirica and Ribatski [50]. Chen et al. [51] investigated flow boiling patterns for R134a in four vertical metallic tubes having inner diameters of 4.26, 2.88, 2.01 and 1.1 mm. They found that the flow patterns in the two largest tubes are similar to those observed in conventional ones. When the diameter was decreased to 2.01 mm, the flow patterns experienced "small tube characteristics" where the liquid film around the long bubble became thinner and the liquid vapour interface in churn flow became less chaotic. Also in the 2.01 mm tube, confined bubbles appeared first at 6 bar system pressure and was established at all pressures 6–14 bar when the diameter was decreased further to 1.1 mm. Since the 2.01 mm tube showed both small tube characteristics and conventional tube characteristics, they concluded that the threshold diameter between small and conventional tubes may be of the order of 2 mm. This value agrees with the value predicted by the first criterion (c1) given by Tibirica and Ribatski [50] and the criterion given by Ong and Thome [48] and is near to the values given by the criterion of Cornwell and Kew [44]. It is worth noting that the values predicted by the two criteria given by Tibirica and Ribatski [50] are completely different. This may be attributed to the fact that they were based on two different ideas and two different flow regimes. This creates another complexity in the identification of the threshold diameter because it seems that there is a threshold for each flow regime. For example, for R-134a based on the absence of stratification effects in plug flow, the threshold was 1.94 mm, while in annular flow, the value was 0.17 mm (see Table 1). Additionally, the dependence of the different criteria on fluid properties and operating conditions make the definition of the threshold diameter very complex. Fig. 6 depicts the effect of saturation temperature on the threshold for R-134a and water.

It is obvious that some criteria demonstrate small dependence on the saturation temperature, while others indicate a strong dependence. In conclusion, a comprehensive definition that considers the fundamental phenomena and mechanism(s) is required to classify normal, small and micro size tubes. More experimental data that consider a wide range of diameters and different fluids are necessary.

4. Flow patterns and heat transfer mechanism(s)

Local heat transfer measurements, combined with flow visualization, can help in the understanding of the dominant flow boiling heat transfer mechanism(s) in microchannels. There is a consensus that reducing the channel diameter results in significant changes in flow patterns. As mentioned above, Chen et al. [51] investigated the effect of tube diameter on flow patterns using R134a and a diameter range of 1.1–4.26 mm. Fig. 7 depicts the flow patterns observed in the larger and smaller tubes. The flow patterns found in the 4.26 mm diameter tube were similar to those observed in the conventional large diameter tubes, namely, dispersed bubble, bubbly, slug, churn, annular and mist flow. By contrast, the flow patterns observed in the 1.1 mm diameter tube demonstrated the following features: (1) the absence of mist flow, (2) the appearance of the confined bubble, (3) the thinning of the liquid film surrounding the vapour slug, and (4) churn flow becoming less chaotic, i.e. there is a tendency for churn flow to diminish as the diameter decreases. Chung and Kawaji [52] did not observe churn flow in 50 and 100 μm diameter tubes and slug flow was the dominant flow pattern. The changes in flow patterns with diameter and operating conditions (pressure, mass flux, heat flux) are expected to affect the local heat transfer mechanism and consequently the heat transfer coefficient. This section sheds some light on the link between flow patterns and heat transfer mechanism(s) in microchannels.

It is well known that the dominant flow boiling heat transfer mechanisms in large diameter channels are nucleate and convective boiling. Nucleate boiling dominates up to intermediate vapour qualities where the flow pattern is bubbly, slug and churn. The enhancement in the heat transfer process due to nucleate boiling arises from the evaporation of the thin liquid film underneath the bubble during its growth period and the strong mixing in the bulk flow due to bubble agitation after the bubble leaves the nucleation site. Based on the fundamentals of pool boiling, the bubble generation frequency, the bubble departure diameter and the diameter range of active nucleating sites increase as the heat flux and pressure increase. Accordingly, the conventional criteria used to infer the nucleate boiling contribution in flow boiling was based on the effect of heat flux and system pressure. It dominates when the heat transfer coefficient increases with heat flux and system pressure but is independent of mass flux and vapour quality. On the other hand, convective boiling dominates at high vapour quality when the flow pattern becomes annular and the nucleation process is nearly suppressed. This mechanism is very similar to the

Table 1
Macro to micro scale transition criteria proposed by different research groups.

Author	Criterion	Macro-to-micro threshold diameter (mm), T_{sat} = 40 °C					
		Water	R134a	R236fa	R245fa	HFE7100	Refrigerant (average)
Suo and Griffith [45]	$D = 0.134La$	0.36	0.1	0.11	0.13	0.133	0.113
Brauner and Moalem-Maron [43]	$D = 2\pi La$	16.8	4.73	4.96	6.1	6.2	5.31
Kew and Cornwell [44]	$D = 2La$	5.34	1.5	1.58	1.93	1.97	1.69
Triplett et al. [46]	$D = La$	2.67	0.75	0.79	0.96	0.99	0.84
Ullmann and Brauner [47]	$D = \sqrt{1.6}La$	3.38	0.95	1	1.22	1.25	1.07
Harirchian and Garimella [49]	$D = \sqrt{(160\mu La)/G}$	0.53	0.14	0.174	0.23	0.32	0.18
Ong and Thome [48], Co = 0.35	$D = 2.94La$	7.86	2.22	2.32	2.84	2.9	2.46
Tibirica and Ribatski [50]criterion 1 (c1)	$D = La\sqrt{8\cos(\theta)}$	6.85	1.93	2.03	2.47	2.53	2.16
Tibirica and Ribatski [50]-criterion 2 (c2)	$D = La\sqrt{1/20}$	0.6	0.17	0.18	0.22	0.22	0.19

Please cite this article in press as: T.G. Karayiannis, M.M. Mahmoud, Flow boiling in microchannels: Fundamentals and applications, Appl. Therm. Eng. (2016), http://dx.doi.org/10.1016/j.applthermaleng.2016.08.063

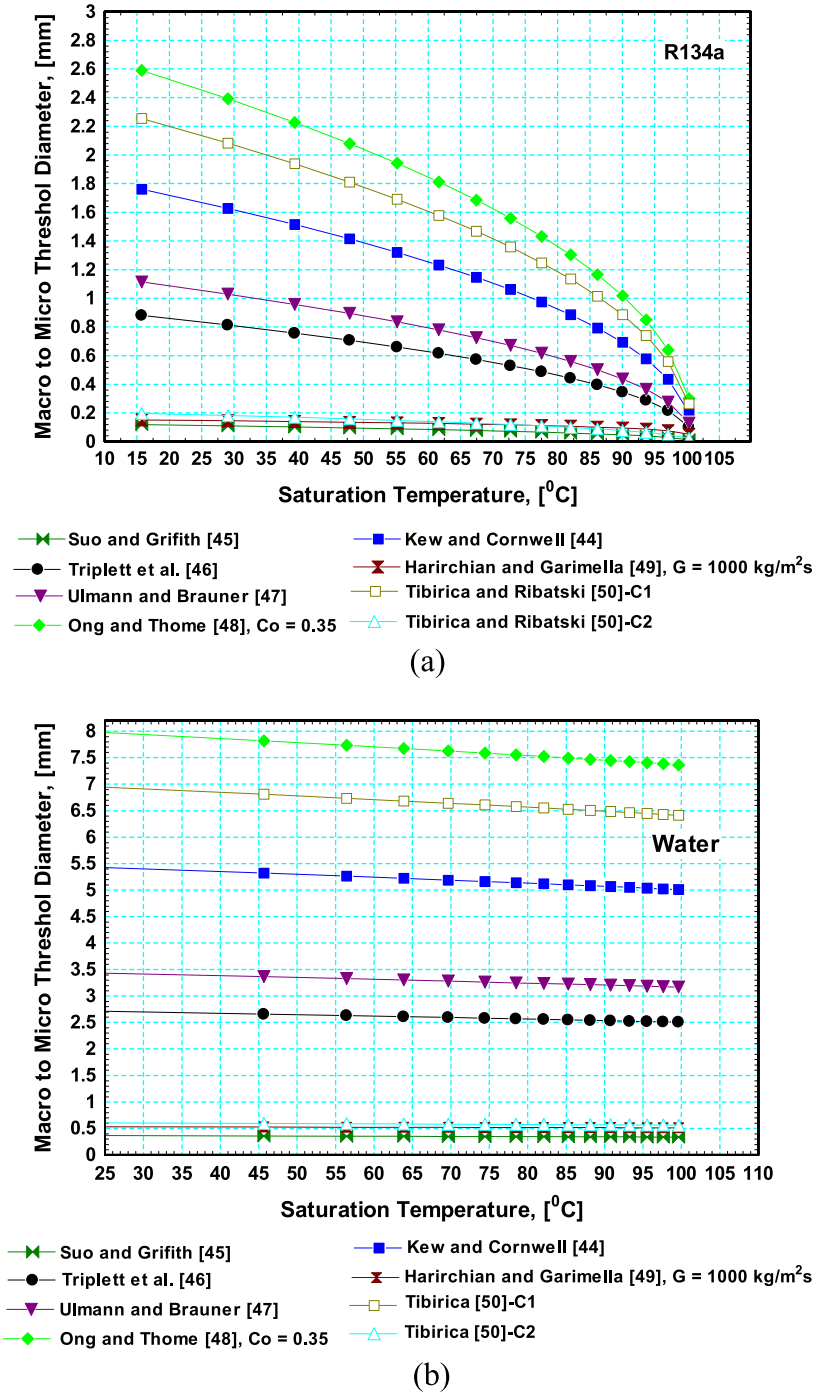

Fig. 6. The effect of saturation temperature on the threshold value for R134a (a) and water (b).

single phase forced convection mechanism but with a certain enhancement factor due to the increase in gas velocity and evaporation of the liquid film. Thus, the conventional criterion used to infer the convective boiling contribution was based on the effect of mass flux and vapour quality (liquid and vapour Reynolds number). It dominates when the heat transfer coefficient increases with increasing mass flux and vapour quality but is independent of heat flux. These criteria have also been applied to flow boiling in microchannels with various conclusions were reached by different research groups. A group of researchers, such as [53,54], concluded that nucleate boiling is the dominant heat transfer mechanism. A second group, such as [55–57], concluded that both nucleate and convective boiling mechanisms contribute to the overall heat transfer process. A third group of researchers, such as [58–60], reported the dominance of the convective boiling mechanism. Some other researchers, such as Huh et al. [61–64], reported that thin film evaporation could be a contributing mechanism. Only one study by Yen et al. [5] reported the suppression of both nucleate and convective boiling mechanisms and attributed the deterioration in heat transfer coefficient in their study to this suppression. Another study by Basu et al. [65] reported that the boiling mechanism was not clear. It is obvious from these studies that there is no common agreement on the dominant heat transfer mechanism(s) in microchannels. Thome and Consolini [66] discussed the mechanisms of boiling in microchannels and summarized the following: (1) nucleate boiling and liquid convection in bubbly flow, (2) liquid

Please cite this article in press as: T.G. Karayiannis, M.M. Mahmoud, Flow boiling in microchannels: Fundamentals and applications, Appl. Therm. Eng. (2016), http://dx.doi.org/10.1016/j.applthermaleng.2016.08.063

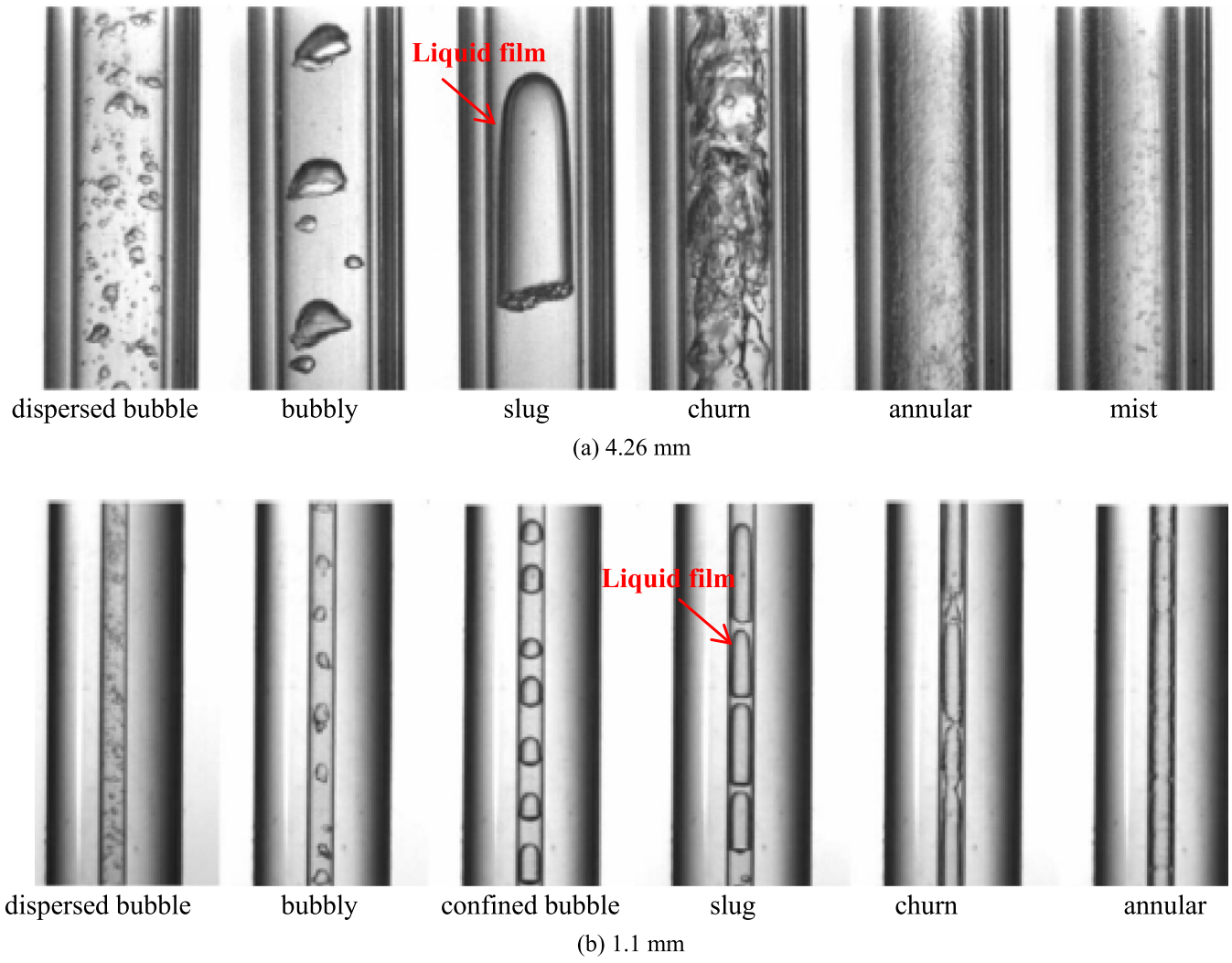

Fig. 7. The flow boiling patterns of R134a at 10 bar in small to mini diameter tubes, Chen et al. [51].

film evaporation and convection to the liquid slugs in slug flow, (3) laminar or turbulent convective film evaporation in annular flow, and (4) vapour heat transfer with liquid impingement in mist flow. They reported that the dependence of the heat transfer coefficient on heat flux is not enough to confirm the dominance of nucleate boiling mechanism. The heat flux effect was attributed to the dependence of the thin film evaporation and bubble frequency on heat flux. Interestingly, they also concluded that the experimentally determined trend in the local heat transfer coefficient versus local vapour quality is a controversial point, because the measured trend does not show the expected increase with quality as would be expected if the dominant mechanism was liquid film evaporation. Accordingly, they recommended investigating the effect of surface roughness and flow regimes on flow boiling mechanism (s). Fig. 8 depicts, in a schematic form, the different mechanisms, which are deemed to be important at the micro scale by the present authors.

Most studies concluded the dominant flow boiling mechanisms, based on the effect of heat flux, mass flux, system pressure and vapour quality. In most studies, flow visualization was conducted at the exit of the heated section, with no detailed information available about the flow patterns inside the heated tube. This makes inferring the mechanism precisely very difficult. Harirchian and Garimella [67,68] conducted an experimental study on flow boiling of FC-77 in silicon multi-microchannels with a fixed depth of 400 μm and widths ranging from 100 to 5850 μm with a mass flux range of 225–1600 kg/m^2 s. Flow visualization was possible through the top transparent cover. Based on heat and mass flux effects, nucleate boiling was found to be the dominant heat transfer mechanism in all cases, except, for channels with width of 100 and 250 μm and mass flux of 250 kg/m^2 s. Accordingly, they concluded that convective boiling is more important as the channel size and mass flux decrease. In other words, channel size affects the heat transfer mechanism. Their flow visualization demonstrated very interesting features that might contribute to understanding the prevailing mechanisms. These features included observing small nucleating bubbles in the liquid slugs between consecutive bubbles and also in the liquid film of wispy-annular flows. When the channel width was decreased to 100 μm, slug flow was established directly after boiling incipience and the small bubbles in the liquid slugs disappeared after a certain heat flux. As the heat flux was increased, the tail of the vapour slug and the liquid film broke up at the locations of nucleating bubbles on the wall. Even in annular flow, bubble nucleation in the film was observed, but it disappeared after a certain heat flux. Borhani and Thome [69] investigated the intermittent dewetting and dryout in annular flow using R245fa and a silicon multi-microchannel evaporator. They also observed small nucleating bubbles in the annular liquid film at a mass flux of 150 kg/m^2 s and 140 kW/m^2, as seen in Fig. 9. The possibility of having small nucleating bubbles in the liquid film

Please cite this article in press as: T.G. Karayiannis, M.M. Mahmoud, Flow boiling in microchannels: Fundamentals and applications, Appl. Therm. Eng. (2016), http://dx.doi.org/10.1016/j.applthermaleng.2016.08.063

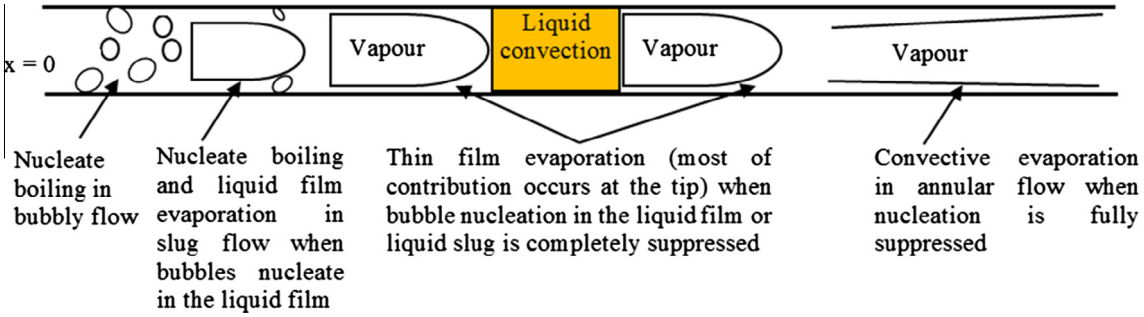

Fig. 8. Schematic drawing for the different mechanisms in flow boiling in small to micro diameter channels.

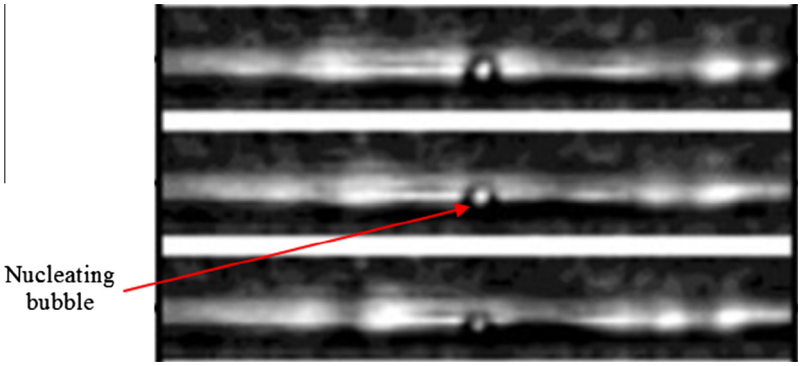

Fig. 9. Nucleation in the annular liquid film, Borhani and Thome [69].

region in slug and annular flows encouraged the question on the contribution of the nucleation compared to thin film evaporation. Kandlikar and Balasubramanian [70] investigated the effect of orientation on flow boiling of water in 1.054×0.197 mm parallel "minichannels". Their flow visualization indicated that there are small nucleating bubbles in the liquid slugs between the elongated bubbles. Also, for downward flow, they observed nucleating bubbles in the thin film around the vapour plug and in the wavy-annular flows. The heat transfer coefficient was found to reach a peak value at near zero vapour quality, then it decreases continuously with increasing vapour quality. This was attributed to the "dominance" of nucleate boiling observed in the bulk liquid in slug flow and in the thin liquid film of annular flow with local dry patches (low heat transfer coefficient) underneath the bubble [70]. It is worth mentioning that the three-zone model of Thome et al. [71] predicts a similar trend although nucleate boiling was assumed to be fully suppressed in their model. Contrary to the above studies, Ali et al. [63] investigated flow boiling of R134a and R245fa in a directly heated quartz tube with a diameter 0.781 mm. They did not observe nucleating bubbles in the liquid film around the elongated bubble. Thus, they concluded that nucleation was suppressed and thin film evaporation is the dominant mechanism in the elongated bubble regime. It is worth noting that, based on the effect of mass and heat flux on the heat transfer coefficient, nucleate boiling is the dominant heat transfer mechanism in their study. However, based on flow visualization, they reported that nucleation was restricted to a region close to the tube inlet (very low vapour quality or bubbly flow) while no nucleation was observed along the rest of the tube. The contradiction between this study and the studies of Harirchian and Garimella [67,68] and Kandlikar and Balasubramanian [70] on observing nucleating bubbles in the liquid film could be due to the following reasons: (1) differences in surface finish, glass versus copper channels, (2) differences in geometry, circular versus rectangular. The presence of channel corners in rectangular channels might assist the nucleation process, and (3) single channel versus multi-channels. In multi-channels, flow reversal and mal-distribution may affect the distribution of the local heat flux and thus the nucleation process. In channels that undergo high instantaneous local heat flux (high wall superheat) activation of nucleation sites may occur.

Bigham and Moghaddam [72] investigated experimentally the mechanisms of heat transfer during flow boiling of FC-72 in a single microchannel at a mass flux of 68.4 kg/m^2 s. The microchannel had 0.3 mm width and 0.075 mm wall thickness. They did not give the channel height. The bottom surface of the channel was made of a composite material consisting of a thick high thermal conductivity silicon layer (0.5 mm thickness) coated with a thin film of a low thermal conductivity material SU8 (9.8 μm thickness). A total of 53 platinum resistance temperature detectors, RTD, were deposited at the fluid-SU8 interface and at the SU8-silicon interface leading to a high resolution measurement of temperature underneath the moving bubble. Flow visualization was synchronized with the temperature measurements at a frame rate of 200,000 f/s. The temperature sensors worked also as a heater, resulting in a heating area of 0.004 mm^2. Additionally, an artificial nucleation site, 0.3 μm in diameter, was created at the centre of the heater using a focused ion beam milling machine. Fig. 10 depicts the typical images of the moving elongated bubble over the heater and the corresponding local instantaneous heat flux. Their results demonstrated that four mechanisms contribute to the heat transfer process in the elongated bubble regime. These mechanisms are: (1) The micro-convection mechanism which occurs during the passage of the liquid slug. The heat flux and the heat transfer coefficient show single phase behaviour. (2) Thin film evaporation (microlayer evaporation). This mechanism starts when the head of the bubble reached the sensor where the heat flux (heat transfer coefficient) increased suddenly to a maximum value then to a plateau with small fluctuations for a while. After this plateau, a rapid decrease in heat flux (heat transfer coefficient) occurred, which was due to the observed partial dryout underneath the bubble. (3) Transient

Please cite this article in press as: T.G. Karayiannis, M.M. Mahmoud, Flow boiling in microchannels: Fundamentals and applications, Appl. Therm. Eng. (2016), http://dx.doi.org/10.1016/j.applthermaleng.2016.08.063

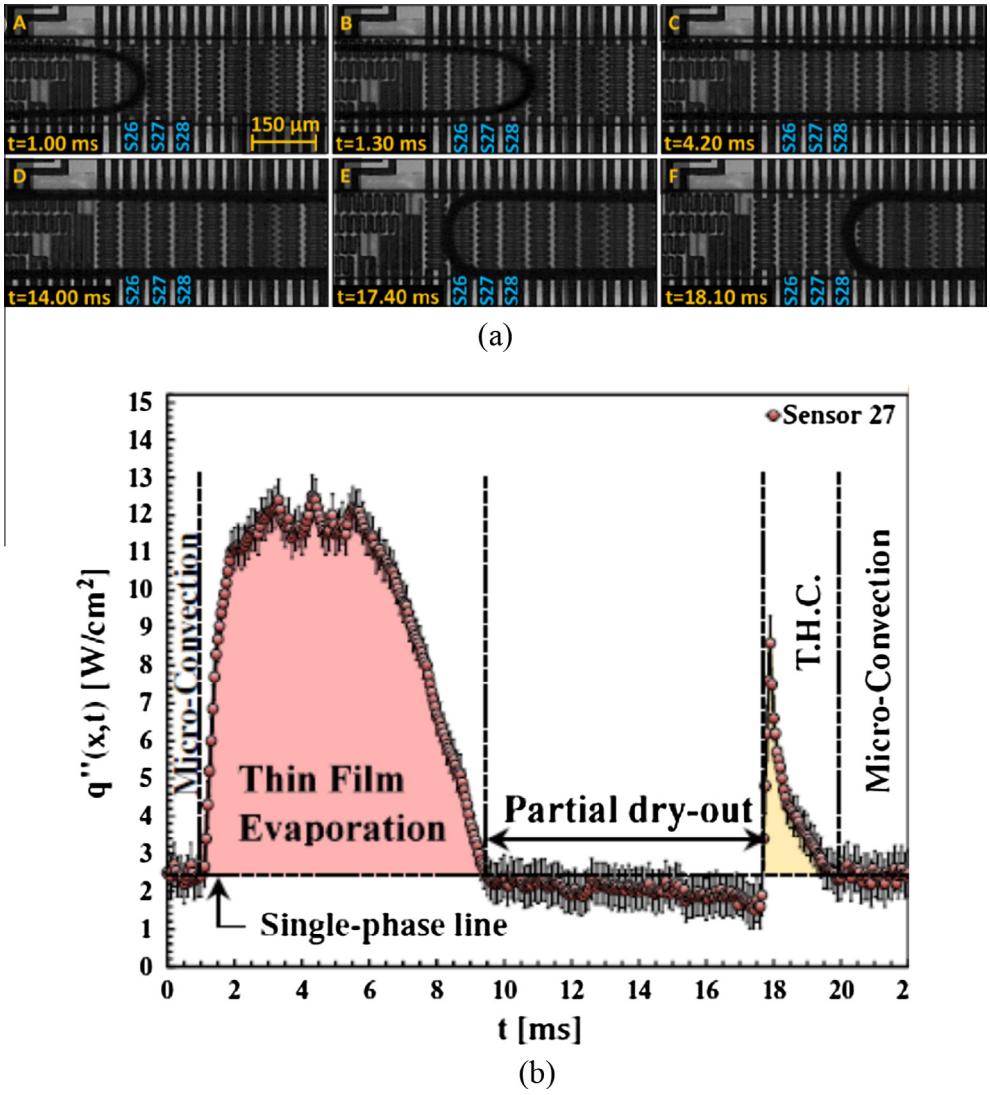

Fig. 10. Motion and growth of the elongated bubble due to evaporation (a) and the instantaneous heat flux and heat transfer mechanisms during the passage of the elongated bubble over the temperature sensor (b), Bigham and Moghaddam [72]; T.H.C. (transient heat conduction).

heat conduction. This mechanism works when the rear of the bubble passes over the sensor and rewets the dry patch underneath the bubble. At this condition, the heat flux and heat transfer coefficient exhibited another jump, without a plateau, followed by a sudden decrease to the steady state single phase value when the liquid slug wets the sensor completely. They reported that this behaviour was similar to the heat flux spikes observed in nucleate pool boiling. It can be concluded, by the present authors, that if thin film evaporation in the elongated bubble regime is similar to the microlayer evaporation in nucleate pool boiling, the heat transfer mechanism can still be assumed as nucleate boiling dominant.

The above studies demonstrate that there is no general consensus on the dominant heat transfer mechanism(s) in microchannels and more experimental studies are required. These studies should cover wide ranges of surface micro structure, fluid properties, mass flux, heat flux and heated length.

5. Flow instability

Flow boiling instability is a critical issue that should be taken into consideration during the design of micro evaporators. It might have a dramatic effect on the overall system performance. Once the flow becomes unstable, all system parameters such as mass flow rate, pressure and temperature oscillate with large amplitudes. These amplitudes can be as high as 36 K for wall temperature, as found by Wang et al. [73], and 992.4 kg/m^2 s and 60 kPa for mass flux and pressure drop, respectively, as found by Fu et al. [74]. Thus, the local time averaged heat transfer coefficient may be strongly influenced by these fluctuations. Understanding the reasons for instabilities may help find solution to this issue. The possible reasons for flow instability can be summarized as follows:

1. Rapid bubble growth and expansion in the upstream and downstream sides of the channel. This explanation was reported by [75–79]. At this condition, it was observed by all the above that the bubble remains stationary for a very short time period with small axial oscillations or slides slowly forward. Accordingly, evaporation of the thin liquid layer underneath the bubble during this period results in the formation of a dry patch, which is responsible for the instantaneous jump in the wall temperature. When the bubble departs and moves away from the nucleation site, fresh liquid wets the surface and the wall temperature drops again.

Please cite this article in press as: T.G. Karayiannis, M.M. Mahmoud, Flow boiling in microchannels: Fundamentals and applications, Appl. Therm. Eng. (2016), http://dx.doi.org/10.1016/j.applthermaleng.2016.08.063

2. Size of outlet section – single channel. This reason was proposed by Qi et al. [76] who investigated flow boiling of liquid nitrogen in four cold drawn stainless steel tubes having diameters of 0.531, 0.834, 1.042 and 1.931 mm. The test sections were connected between two plenums with diameters larger than the test section diameter, i.e. inlet and outlet restrictions. They attributed the instability observed in their experiment to the effect of the outlet restriction (outlet plenum) and they explained it as follows: after boiling incipience, small bubbles move downstream and enter the outlet plenum, where their velocity decreases due to the sudden area enlargement. As a result, more bubbles accumulate inside the plenum, resulting in the formation of a large vapour patch, which can cause a temporary blockage. This blockage leads to a sharp decrease in mass flux, which in turn results in an increase in the wall temperature and vapour quality. The sudden increase in vapour quality, due to the reduction in mass flow rate, results in a sudden peak in pressure drop. Once the vapour patch passes through the outlet restriction, fresh liquid enters the tube and the mass flux increases again, improving the heat transfer process and reducing wall temperature.
3. Inlet compressibility effects, as presented in [80–83]. Yan and Kenning [80] observed that, for high inlet compressibility, the confined bubble grows axially in the upward and downward directions simultaneously, until it reached the channel inlet. At low inlet compressibility, the lower end (upstream) of the growing bubble was found to remain almost stationary. Gedupudi et al. [81] investigated the effect of inlet compressibility during flow boiling of de-ionized water in a single copper channel of $0.38 \times 1.6 \times 40$ mm and 7 K inlet sub-cooling. The effect of inlet compressibility was investigated by creating subcooled boiling in the preheater located ahead of the test section. It was observed, for both compressible and incompressible inlet conditions, that bubbles nucleate at a certain location then grow over a short period to the size of the shortest dimension (0.38 mm) then grow over a longer period to the size of the largest dimension (1.6 mm). In the case of no inlet compressibility and after the bubble becomes confined, the bubble grows only in the downstream direction, while with inlet compressibility, it grows both in the upstream and downstream directions. Gedupudi et al. [82] presented a 1-D model to study the effect of inlet resistance on flow reversal for different initial upstream compressible volumes. It was found that, for a fixed upstream compressible volume, as the inlet resistance increased, the maximum flow reversal distance decreased (the distance travelled by the bubble in the upstream direction). They reported an optimum value of 20 for the pressure loss factor ($\Delta P_{restrictor}/0.5\rho U_{ch}^2$) across the inlet restriction, after which there is no significant effect. Liu et al. [83] studied flow boiling of water and *n*-hexane in brass and copper tubes, 0.9 and 2 mm in diameter and 270 mm in heated length for a mass flux range of 60–180 kg/m^2 s, a heat flux range of 20–465 kW/m^2, a pressure range of 100–200 kPa, an inlet temperature range of 20–50 °C and a vapour quality range of 0–0.8. They used a buffer reservoir before the test section inlet to investigate the effect of inlet compressibility. They used the term "hard inlet" to describe the condition when the buffer reservoir was full of liquid (no buffer reservoir) and the term "soft inlet" when the amount of gas in the reservoir was varied to give inlet conditions with a known compressibility. The results demonstrated that, for the hard inlet at 0.15 exit quality, the inlet pressure fluctuates irregularly with ±2.1 kPa rms and a frequency of 6–10 Hz while the flow rate remained steady. For the soft inlet condition, the flow rate and inlet pressure exhibited periodic in-phase oscillations with a frequency of 2.2 Hz. It was concluded that, as the buffer volume increases, the amplitude and frequency of the oscillations decreases. For the hard inlet conditions, the local heat transfer coefficient peaked at $x \approx 0$, then decreased to a plateau up to $x \approx 0.6$, while for the soft inlet, the heat transfer coefficient did not decrease after its peak. Instead, it shows a plateau immediately and the heat transfer coefficient was about 30% higher compared to the hard inlet conditions.
4. Nucleation near the channel inlet. Kandlikar [84] discussed nucleation and instability in microchannels and reported that the location of boiling incipience affected flow reversal, and thus the oscillation in the measured parameters such as pressure and temperature. When nucleation occurred near the channel exit, the flow resistance in the back flow direction increased and consequently no flow reversal occured (stable flow). On the contrary, when nucleation occurred near the channel inlet, the flow resistance in the backflow direction decreased and thus flow reversal occurred (unstable flow).

An example of flow reversal in microchannels was given by Fayyadh et al. [85]. They investigated flow boiling of R134a in a copper, multi-microchannel evaporator having a 0.3 mm channel width, a 0.7 mm channel height, a 0.2 mm fin thickness and a 20 mm channel length. The channels were cut on the top of a copper block, while the manifold and plenum were cut in the polycarbonate housing block. The fluid entered the channels through a deep plenum and a manifold with a convergent cross sectional area and the same depth as the channel. It left the channel through a manifold with a divergent cross section area into a deep outlet plenum. The mass flux ranged from 50 to 300 kg/m^2 s. It was found that, for G = 50 kg/m^2 s, flow reversal occurred at boiling incipience and continued for all heat fluxes. Fig. 11 shows the sequence of pictures for flow reversal occurring at boiling incipience for P = 6.5 bar and G = 50 kg/m^2 s. It is obvious from the pictures that the vapour patch stays for about 210 ms in the inlet manifold, with back and forth motion, before its rupture into segmented bubbles that moved downstream. As the mass flux increased, the heat flux at which flow reversal occurred increased. Very mild flow reversal was observed in the inlet manifold at a base heat flux of 149 kW/m^2 for G = 300 kg/m^2 s, where the vapour patch stayed only for about 10 ms in the inlet manifold.

A number of researchers, such as [86,87], proposed inserting a flow restrictor at the channel inlet, while some other researchers proposed channels of expanding cross section to reduce flow instability. Koşar et al. [86] used a rectangular orifice with a fixed width of 20 μm and a variable length at each channel inlet. It was found that as the ratio of the pressure loss in the inlet restrictor to the major pressure loss across the channel increased, the heat flux at which the flow become unstable increased asymptotically. It is interesting to note that, although the flow was deemed stable with the inlet restrictor, the surface temperature reached a value of about 180 °C at G = 389 kg/m^2 s. This value is very high if this heat sink is to be used for electronics cooling. It is not clear whether this high surface temperature is linked to the inlet restrictor or not. Kuan and Kandlikar [87] reported that the heat transfer rate and flow stability were improved for channels with inlet restrictions compared to channels without restrictors. In their testing module, each channel was connected to the inlet manifold through a 0.127 mm diameter hole which represented 6.1% of the channel cross section area. However, inspecting their results, one can see that the inlet restrictor reduced the surface temperature by about 1 K for the same heat flux. In other words, the enhancement in the heat transfer coefficient was about 11%, which was comparable to the experimental uncertainty. Lu and Pan [88] tested channels with a diverging cross section. They reported that mild flow reversal was observed in some of the channels at stable flow conditions

Please cite this article in press as: T.G. Karayiannis, M.M. Mahmoud, Flow boiling in microchannels: Fundamentals and applications, Appl. Therm. Eng. (2016), http://dx.doi.org/10.1016/j.applthermaleng.2016.08.063

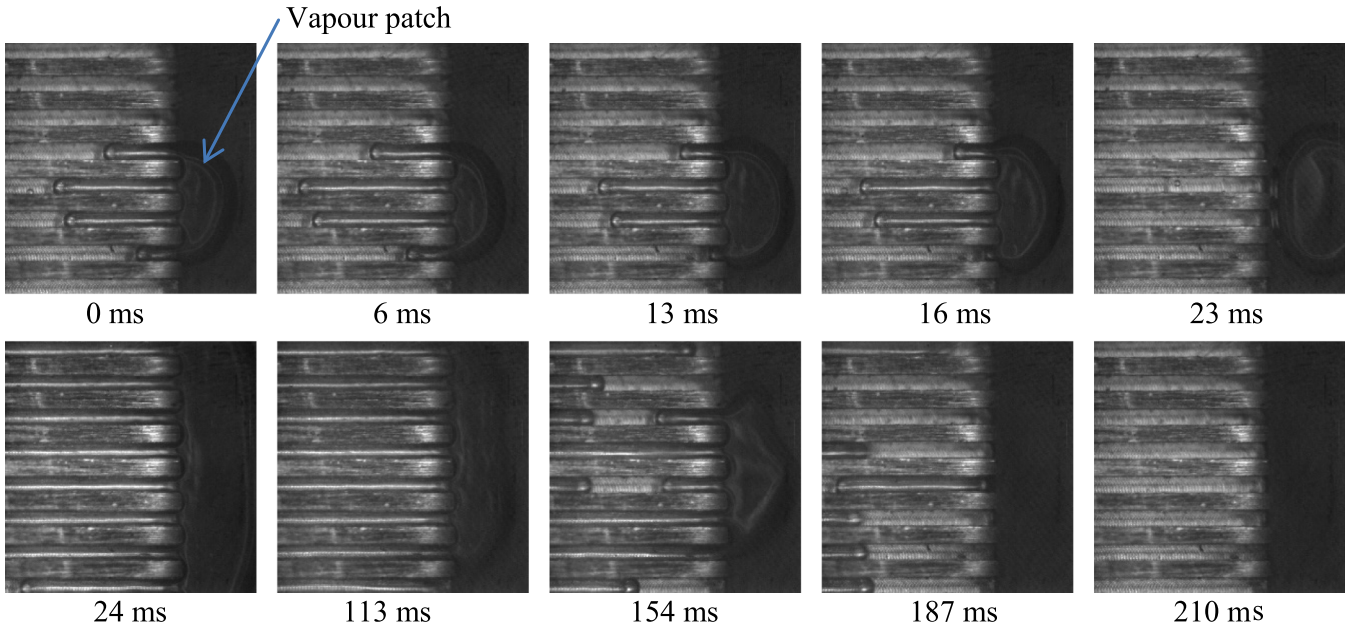

Fig. 11. Sequence of pictures for flow reversal observed at G = 50 kg/m^2 s, P = 6.5 bar and R134a, Fayyadh et al. [85].

and was attributed to the high wall superheat at boiling incipience. This resulted in rapid bubble growth. Tamanna and Lee [89] investigated flow boiling instability of de-ionized water in an expanding silicon micro-gap heat sink of 12.7 × 12.7 mm. Three micro-gaps were investigated including, a straight micro-gap of depth 0.2 mm, expanding micro-gap with the same inlet depth of 0.2 mm and gradually increasing exit depths of 0.3 and 0.46 mm. They concluded that the amplitude of the inlet pressure oscillation decreased by about 50% in the expanding micro-gap with a 0.3 mm outlet depth, compared to the straight micro-gap. In contrast, increasing the outlet depth further to 0.46 mm resulted in higher oscillation amplitudes. In addition, flow reversal at the inlet plenum was reported, even in the expanding micro-gap that was deemed to reduce flow instability.

Other possible reasons of flow instabilities are suggested by the present authors and can be summarized as follows:

1. Channel surface characteristics. This factor was ignored by many researchers when they presented and discussed their flow instability results. If the boiling surface is very smooth (very limited number of nucleation sites), high wall superheat will be required to start boiling. This will result in a highly superheated liquid (unstable phase), which will result in a very rapid bubble growth (like explosive boiling) immediately after phase change and consequently large oscillations in pressure and temperature. Accordingly, using microchannels with surfaces that have a sufficient number of nucleation sites could help reduce the flow instability encountered at boiling incipience.
2. Using surfactants can affect bubble nucleation and thus the thermal instabilities induced by boiling incipience. It can reduce the bubble departure diameter and the nucleation period, as reported by King and Sadhal [90]. In other words, the bubble may depart quickly before the formation of dry patches underneath the bubble. This reduces the cyclic variations in surface temperature.
3. The surface wettability. According to the correlation of Fritz, cited in Collier and Thome [91], the bubble departure diameter in pool boiling increases as surface tension and contact angle increase (increasing surface wettability). For example, for water at 40 °C saturation temperature and a contact angle of 650, the departure diameter is 3.6 mm, which is very large compared to the microchannel size. In contrast, for R134a at the same saturation temperature, the departure diameter is 0.55 mm (more than six times smaller). These values are an order of magnitude different and are given here only for comparison because the bubble size is expected to be different in flow boiling. This may explain why all researchers who used water as the test fluid reported severe flow instability while researchers who used refrigerants did not report the instability issue. For instance, the present authors conducted a flow boiling study using R134a in a 1.1 mm diameter vertical tube and did not see any instability except at very high heat fluxes, when dryout occurred, see [92,93]. The large bubble departure diameter means that the bubble becomes confined before it leaves the nucleation site (stationary and elongated bubble). This could result in local dry patches underneath the bubble and consequently severe oscillations in the local surface temperature. Also, the periodic blockage of the channel with a stationary elongated bubble could result in severe oscillations in the inlet pressure.
4. Channel thermal conductivity or the conjugate effect. This factor may explain the instabilities reported in all studies that used silicon and copper multi-microchannels. Most silicon channels mentioned in the literature are manufactured by the lithography technique, where the inlet and outlet manifolds are integrated. The high thermal conductivity results in uniform surface temperature distribution (isothermal surface). Thus, nucleation may occur at locations very near to the channel inlet, or even in the inlet manifold, at high heat fluxes and consequently large oscillations in the inlet pressure could occur. Thus, the effect of channel material should be investigated further in order to understand the conjugate effects.
5. The size of the inlet/outlet manifold in multi-channels configuration. Most previous studies did not provide any details on the size of the inlet/outlet manifolds or plenums. The design of a multi-channel heat sink with a large outlet manifold and very small exit tubing could result in flow instability, particularly as the mass flux increases. Fig. 12 shows the test sections used by some researchers who reported significant flow instability

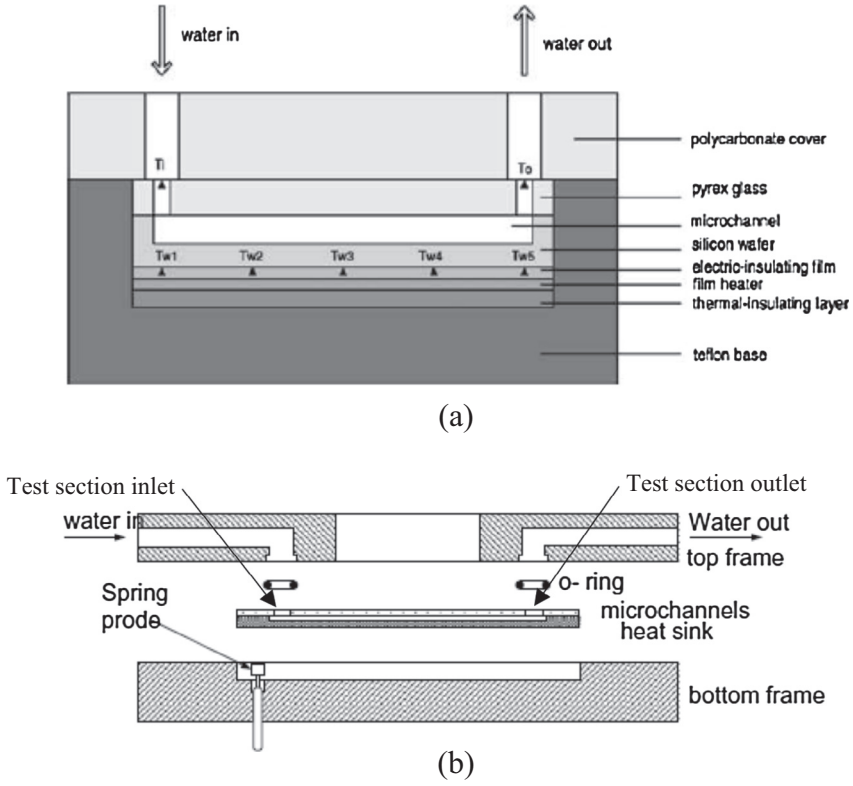

Fig. 12. The test sections design used by (a) Wang et al. [73] and (b) Bogojevic et al. [77].

such as Wang et al. [73] and Bogojevic et al. [77]. As seen in the figure, the flow entered and left the test section through a very small hole drilled in the glass top layer. The instability arose from trapped vapour accumulation inside the manifold, which increased the outlet pressure and caused negative pressure drop in the channel. This means that the outlet manifold and connection tubing should be designed such that vapour cannot accumulate inside the manifold. The accumulation of the vapour in the outlet manifold may result in dryout at very low vapour quality, particularly as the mass flux increases.

In summary, several parameters can result in flow instabilities in microchannels. Some researchers reported that flow instabilities can be reduced by inserting flow restrictors at the channel inlet or using channels with a diverging cross sectional area or, as the present authors propose, by modifying the inlet and outlet manifolds. However, the results discussed above, indicated that the effect of instabilities on heat transfer rate is not necessarily significant. In other words, unstable flow may not always give lower the heat transfer rates compared to stable flow.

6. Effect of surface characteristics

This section reviews some of the experimental studies that focused on the effect of surface characteristics in flow boiling in microchannels in order to explain their importance. It is understood that surface characteristics play a significant role in pool boiling, while in flow boiling at the micro scale, there are no rigid conclusions on the effect of channel surface finish. Some researchers such as Jones and Garimella [94] and Alam et al. [95] used the average surface roughness (Ra) as a parameter to investigate the effect of surface characteristics on flow boiling in microchannels. Jones and Garimella [94] investigated the effect of surface roughness on flow boiling in copper multi-microchannels heat sinks. Each heat sink consisted of 10 square channels (0.5 × 0.5 mm) with 25.4 mm channel length. The channels of the first heat sink were manufactured by saw blade cutting, resulting in an average roughness (Ra) value of 1.4 μm. The second and third heat sinks were also manufactured by saw blade cutting, but were then roughened using electrical discharge machining (EDM), resulting in Ra of 3.9 μm and 6.7 μm, respectively. De-ionized water was used as the test fluid over a mass flux range of 200–1000 kg/m^2 s, heat flux up to 3 MW/m^2, a vapour quality range of 0.164–0.464 and 87 °C fluid inlet temperature. They reported that surface roughness had minor effects on the critical heat flux and the wall superheat at boiling incipience. However, the heat transfer coefficient was enhanced by 20–35% for the two EDM roughened surfaces at heat fluxes greater than 1500 kW/m^2, while there was no clear effect at low heat fluxes. Alam et al. [95] studied the effect of surface roughness on flow boiling of water in silicon micro gaps with different surface roughness. The dimensions of the test piece were 12.7 mm width, 12.7 mm length and gap heights 0.5, 0.3 and 0.2 mm. The Ra value was 0.6, 1 and 1.6 μm. Experimental conditions included two mass fluxes of 390 and 650 kg/m^2 s, heat fluxes up to 850 kW/m^2 and 91 °C fluid inlet temperature. It was observed that, for the micro gap with a smooth surface (Ra = 0.6 μm), few bubbles nucleate and slide over the surface without coalescence and confinement. On the contrary, more bubbles were observed in the gaps with Ra values of 1 and 1.6 μm, with coalescence into vapour slugs. They attributed this behaviour to the activation of more nucleation sites in the rougher surfaces. From the boiling curves published in their paper, one can see that the wall superheat at boiling incipience decreased by about 50% when the Ra value was increased from 0.6 to 1 μm. Increasing the roughness further to 1.6 μm did not show any effect. This means that surface roughness affects boiling incipience. Although they concluded that the heat transfer coefficient was higher for the rough surface, the figures presented in their study did not show

a clear effect (the difference seems to be within the experimental uncertainty).

In an attempt to explain the reasons of discrepancies in flow boiling results in small to micro diameter tubes, Mahmoud et al. [92] and Karayiannis et al. [93] investigated flow boiling heat transfer of R-134a in two tubes, 1.1 mm in diameter and 150 mm in heated length. The two tubes were made of stainless steel and were manufactured by two different methods. The first tube was "cold drawn" (manufactured by extrusion and drawn processes) while the second tube was "welded" (manufactured by rolling a strip of metal into the required diameter and then joining the two edges by welding). Experimental conditions included a mass flux of 300 kg/m^2 s, 8 bar system pressure, 5 K inlet sub-cooling and vapour quality up to 0.9. They examined the inner surface of the tubes using SEM analysis. The SEM images are shown in Fig. 13. The images depicted that the surface of the welded tube was smooth, with the presence of some debris on the surface. The measured *Ra* value for this tube was found to be 0.52 μm. By contrast, the SEM image of the cold drawn tube indicated that there were random scratches or channels that seem to be uniformly distributed over the surface. The measured *Ra* value for this tube was 1.27 μm. They reported a peculiar heat transfer behaviour for the welded tube, compared to the cold drawn tube, see Fig. 14. In the welded tube, for each heat flux, the local heat transfer coefficient shows a very high peak at boiling incipience (vapour quality near zero) followed by a sharp decrease then a rapid increase before it decreases again at the last thermocouple location. In other words, the heat transfer coefficient varies significantly along this tube. The existing design correlations cannot predict this peculiar behaviour and may result in inaccurate design of a tubular heat exchanger if welded tubes are used. On the contrary, the heat transfer coefficient in the cold drawn tube exhibited a lower peak at boiling incipience followed by a little variation with vapour quality. It is worth mentioning that the researchers reached the same conclusion when the local heat transfer coefficient was also plotted versus axial distance. The behaviour of the heat transfer coefficient in the welded tube was attributed by Mahmoud et al. [92] to the smooth surface of this tube, with the presence of a few nucleation sites that were not uniformly distributed along the tube, i.e. these sites can produce the peaks seen in Fig. 14a. By contrast, the surface of the cold drawn tube, as seen in the SEM images, depicted large number of nucleation sites (the random scratches on the surface) that looked uniformly distributed along the tube. This may explain the small variations in the local heat transfer coefficient along the tube. There was no significant effect on flow patterns, except at the lowest heat flux where the first bubbles appeared at lower heat flux in the cold drawn tube compared to the welded tube.

Pike-Wilson and Karayiannis [96] used the same experimental facility as Mahmoud et al. [92] and investigated the effect of tube material on flow boiling of R-254fa in three metallic tubes having a 1.1 mm diameter and 300 mm heated length. The selection of tubes with different materials could result in different surface finish and thus different heat transfer behaviour. The investigated

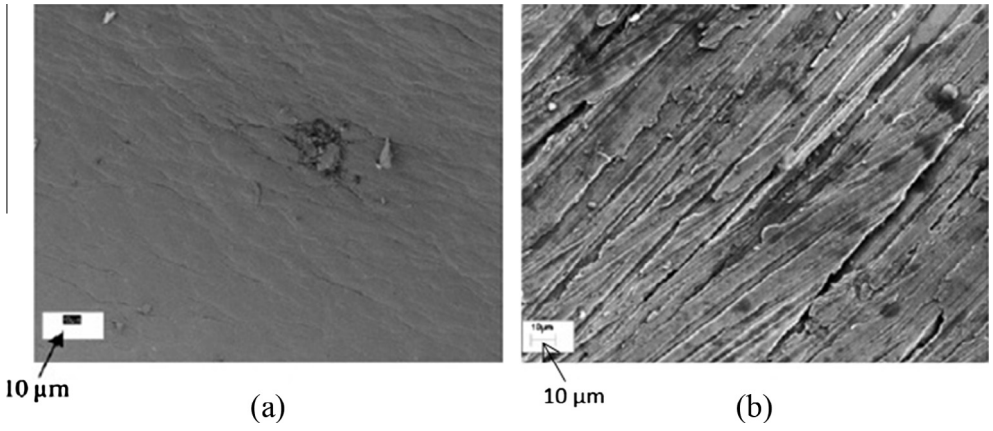

Fig. 13. The SEM images of the stainless steel: (a) welded tube (b) cold drawn tube, Karayiannis et al. [93].

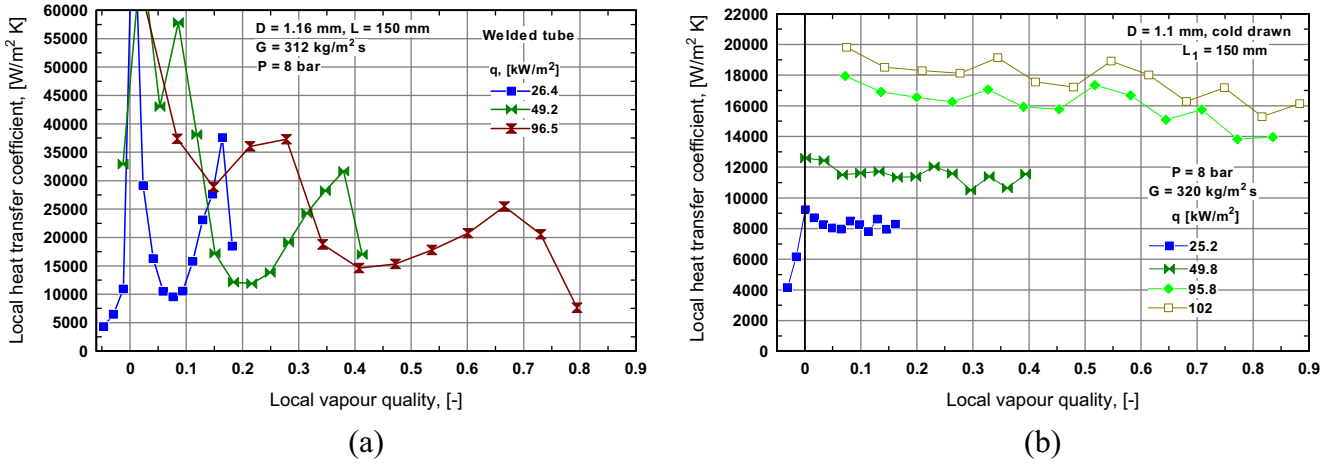

Fig. 14. The local heat transfer coefficient versus local vapour quality for (a) the welded tube and (b) the cold drawn tube, adapted from Karayiannis et al. [93].

Please cite this article in press as: T.G. Karayiannis, M.M. Mahmoud, Flow boiling in microchannels: Fundamentals and applications, Appl. Therm. Eng. (2016), http://dx.doi.org/10.1016/j.applthermaleng.2016.08.063

tubes were manufactured by the cold drawn process and made of stainless steel, copper and brass. Experimental conditions included mass flux range 100–400 kg/m^2 s, heat flux range 10–60 kW/m^2, exit quality range 0–0.95 and inlet pressures of 1.8 and 2.4 bar. They presented a detailed discussion on the methods of roughness measurement, roughness data processing and roughness parameters. It was concluded that the method of surface analysis and data processing could result in different surface data and this should be taken into account by the research community. The inner surface of the three tubes was examined using SEM analysis and the images are shown in Fig. 15. The surface of the stainless steel tube indicated some deposits. The chemical analysis of these deposits showed that it was not a foreign material but it seems to be a result of the manufacturing process. The surface of the brass tube was found to have a flaky structure with horizontal cracks and surface imperfections while the surface of the copper tube shows a smooth structure with "scratches" compared to the stainless steel and brass tubes. The *Ra* values were 1.25 μm for the brass tube, 0.72 μm for the stainless steel tube and 0.52 μm for the copper tube. The flow patterns were reported to be the same in the three tubes where annular flow was the dominant flow regime. Only small differences were reported at low heat fluxes, where slug flow was observed in the brass and copper tubes while annular flow was established in the stainless steel tube immediately after boiling incipience. The heat transfer results, presented as a local heat transfer coefficient versus local quality in Fig. 16, demonstrated that the magnitude and trend were similar for brass and stainless steel tubes with only a small difference; the heat transfer coefficient in the stainless steel surface shows local peak at the fifth thermocouple location. This was attributed by Pike-Wilson and Karayiannis [96] to the local flaws or scratches on the surface, which could form a nucleation site. The heat transfer coefficient in the copper tube was lower and did not show the increasing trend observed in the stainless steel and the brass tubes. It was also reported that, for a fixed heat and mass flux and for $x < 0.35$, there was no clear effect of surface characteristics, while for $x > 0.35$, the heat transfer coefficient was higher for the rough tube (brass) and low for the smooth tube (copper). This behaviour was not observed for all mass fluxes and system pressures. Since the three tubes were manufactured using the same method, the difference in surface characteristics were thought to be due to the material. There is no clear link between the surface roughness and the changes in the heat transfer coefficient and thus the tube material does not have a significant effect on the heat transfer coefficient. It is worth noting that the SEM image of the cold drawn stainless steel tube conducted by Mahmoud et al. [92] in Fig. 13b looks different compared to the SEM image conducted by Pike-Wilson and Karayiannis [96], Fig. 16. This raises another question about the possibility, or not, that the same manufacturing technique produces tubes with a repeatable surface finish.

Cikim et al. [97] investigated the effect of micro tube surface characteristics on sub-cooled flow boiling of de-ionized water. The surface characteristics were changed by nano-coating that had a cross-linked structure. Three tubes (material was not reported) of inner diameter 249 μm, 507 μm and 908 μm were used and the coating thickness was varied (50 nm, 100 nm and 150 nm). The experiments were conducted at two mass flux values of 5000 and 20,000 kg/m^2 s. The researchers did not report on the characterization of the examined surfaces. It was found that the critical heat flux and heat transfer coefficient increased as the coating thickness increased. The maximum enhancement was reported for the smallest diameter tube (249 μm) and the 150 nm coating thickness. For example, the enhancement in critical heat flux at G = 5000 kg/m^2 s was 20.4% for D = 249 μm, 10.1% for D = 507 μm and 8.9% for D = 908 μm compared to the uncoated surface, while the corresponding values at G = 2000 kg/m^2 s were 29.7%, 26% and 23.1%. The enhancement in the local heat transfer coefficient for a given heat flux at G = 5000 kg/m^2 s was 97.4% for D = 249 μm, 85% for D = 507 μm, and 77.1% for D = 908 μm while these values were 126.2%, 90.1% and 86.4% for G = 20,000 kg/m^2 s. They attributed the enhancement in critical heat flux to the decrease in contact angle as the coating thickness increases (improved surface wettability, see below) although they did not report on the measured contact angle for the three investigated surfaces. The enhancements in heat transfer coefficient were attributed to the increased number of nucleation sites, increased bubble generation frequency and improvement of liquid replenishment to the surface, resulting from the cross-linked porous structure of the coating.

It can be concluded from the above studies that the micro structure of the channel inner surface has a significant effect on the local heat transfer rate in microchannels. However, it is very difficult to quantify or relate this effect to the actual heat transfer rates. This is because most researchers use the average roughness to characterize the surface, which may not be the most appropriate parameter, or describes only partially the surface structure in relation to boiling. This may explain the fact that some researchers reported a significant effect of surface roughness while others only a minor effect. A significant research effort is required to design a surface with a known microstructure; then be able to vary this structure and carry out experiments to document the effect on heat transfer rates.

7. Effect of surface wettability

Some researchers investigated the effect of surface wettability (contact angle) on flow boiling in microchannels. Fig. 17 depicts a schematic drawing for the definition of the contact angle which was used to identify the surface wettability. The wettability of

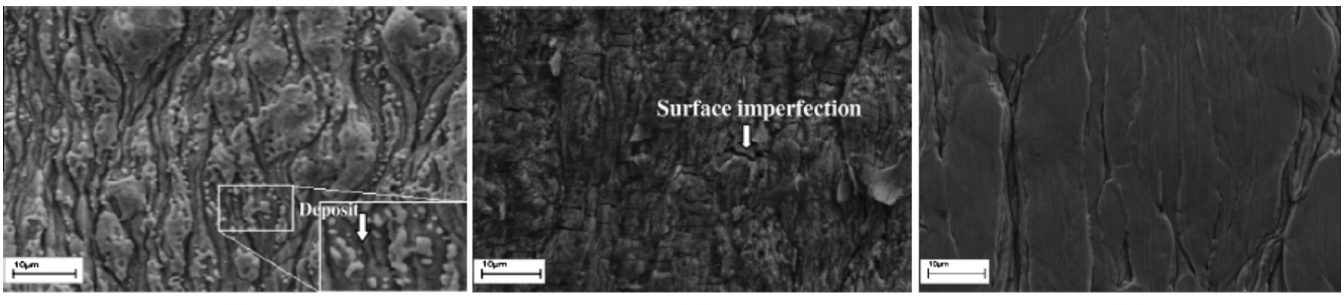

Fig. 15. The SEM images of (a) the stainless steel tube, (b) the brass tube, and (c) the copper tube, Pike-Wilson and Karayiannis [96].

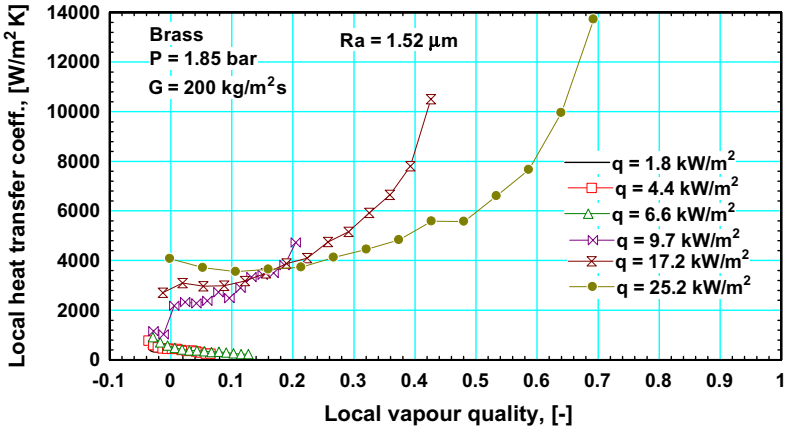

(a)

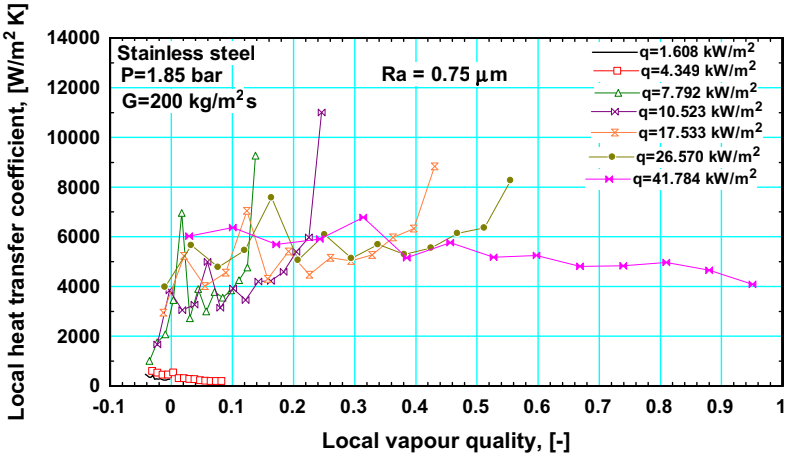

(b)

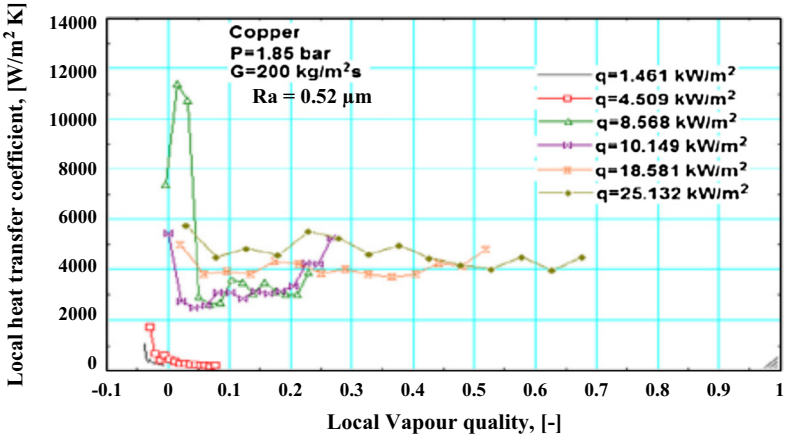

(c)

Fig. 16. The local heat transfer coefficient versus local vapour quality for (a) brass tube, (b) stainless steel tube, and (c) copper tube, Pike-Wilson and Karayiannis [96].

the surface was modified using several coating techniques and different materials. For example, Liu et al. [98] studied the effect of channel surface wettability on flow boiling incipience of water in a single silicon microchannel. The surface wettability was varied by the following methods: (1) Manufacturing the channel by plasma (dry) etching on a silicon wafer, which resulted in a hydrophilic surface with contact angle $\Theta = 36°$. The contact angle was measured by placing a droplet of water on the surface. (2) Coating the bottom surface of the channel with a low surface energy material (perfluoro decyltrichlorosilane) resulting in a hydrophobic surface with $\Theta = 103°$. (3) Coating the surface with silicon nano-wire arrays resulting in a super-hydrophilic surface with $\Theta \approx 0°$. The dimensions of the channel were 105 µm deep, 1000 µm wide and 30 mm long. The heat flux was varied from 230 to 354.5 kW/m^2 and the mass flux from 50 to 583 kg/m^2 s. They reported that, for the super-hydrophilic surface ($\Theta \approx 0°$), large numbers of small

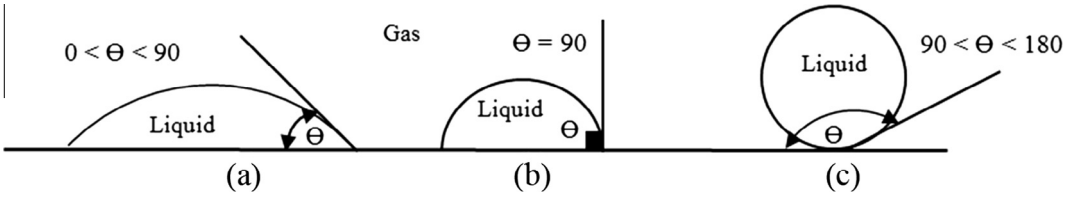

Fig. 17. Schematic drawing for the definition of contact angle and wettability; (a) wetting surface (hydrophilic), (b) non-wetting, and (c) highly non-wetting (hydrophobic).

bubbles was observed to nucleate without coalescence at boiling incipience. On the hydrophilic surface ($\Theta \approx 36°$), bubbles were observed to nucleate, grow and coalesce into elongated bubbles and were flushed periodically by the liquid water entering the channel. For the hydrophobic surface ($\Theta = 103°$), small bubbles were not observed frequently, as was the case in the hydrophilic surfaces. Instead, elongated bubbles formed immediately at boiling incipience. Boiling was found to start at slightly higher heat flux on this surface compared to the hydrophilic surfaces (301 kW/m^2 compared to 280 kW/m^2). This resulted in a highly superheated liquid and thus rapid bubble growth resulting in the formation of elongated bubbles immediately after boiling incipience. Accordingly, they concluded that the bubble detachment diameter in hydrophobic surfaces seems to be larger than that in hydrophilic surfaces.

Choi et al. [99] investigated the effect of surface wettability on flow boiling of water in a single rectangular channel of 50 mm length, 0.5 mm hydraulic diameter and 503 by 507 μm cross section. The channel was made of photosensitive glass, which is a hydrophilic surface with a contact angle of 25°. The surface was coated by octadecyltrichlorosilane to change it into a hydrophobic surface with a contact angle of 105°. The experimental conditions included two mass flux values of 25 kg/m^2 s and 75 kg/m^2 s, a vapour quality range of 0–0.3 and heat flux range of 10–430 kW/m^2. The heat transfer coefficient in the hydrophobic channel was reported to be lower than that in the hydrophilic channel for $x < 0.2$ at G = 25 kg/m^2 s, while the opposite occurred at higher qualities. For G = 75 kg/m^2 s, the heat transfer coefficient in the hydrophobic channel was higher than that in the hydrophilic channel for the whole range of vapour quality. Additionally, for the two mass fluxes, the vapour quality at which dryout occurred in the hydrophobic channel was higher than that in the hydrophilic channel. It was also reported that only few bubbles nucleated and grew into elongated bubbles with a stable liquid film around the bubble in the hydrophilic channel. By contrast, more bubbles were observed to nucleate over the hydrophobic surface without departure from the surface, resulting in local dry patches at low vapour quality. At high vapour quality, elongated bubbles were formed with an unstable liquid film around the elongated bubble. It is interesting to note that they reported nucleation in the unstable liquid film in the hydrophobic channel at high vapour quality. Phan et al. [100] investigated the effect of surface wettability on flow boiling heat transfer of water in a single rectangular channel with a hydraulic diameter of 0.96 mm (5 mm width by 0.5 mm height) and 180 mm length. The channel was made of a Pyrex wafer and the surface wettability was changed by the deposition of nanoparticles, namely: silicone oxide SiO_x ($\Theta = 26°$), titanium Ti ($\Theta = 49°$), diamond-like carbon DLC ($\Theta = 63°$) and carbon-doped silicon oxide SiOC ($\Theta = 104°$). The experimental conditions included mass flux of 100 kg/m^2 s, a heat flux range of 30–80 kW/m^2 and a vapour quality range of −0.1 to 0.2. The heat transfer results obtained by Phan et al. demonstrated that, for all surfaces, the heat transfer coefficient increased to a maximum at a vapour quality less than about 0.015, before decreasing with quality. It is worth mentioning that the highest vapour quality in their study was less than 0.06. The more hydrophilic surface ($\Theta = 26°$) resulted in a lower heat transfer coefficient that had little dependence on vapour quality and heat flux. In contrast, separate lines indicating a clear heat flux effect was found for the other surfaces ($\Theta = 49°, 63°, 104°$). The researchers reported that bubbles were observed on the hydrophobic surface ($\Theta = 104°$), even at negative vapour quality. They attributed this phenomenon to the large amount of gas trapped inside the cavities (non-wetting surface). Therefore, rapid bubble coalescence occurred and resulted in the formation of elongated bubbles with local dry patches that resulted in the deterioration of the heat transfer rate (after the peak value) in the hydrophobic channel. On the other hand, the deterioration of the heat transfer rate in the hydrophilic channels with $\Theta = 49°, 63°$ (decrease in the heat transfer coefficient after the peak value) was attributed by Phan et al. [100] to the dominance of capillary effects that keep the liquid film thickness partially unchanged as vapour quality or heat flux increased. Additionally, the wall superheat at boiling incipience was found to decrease as the contact angel increases, which agrees with Liu et al. [98].

Sujith et al. [101] investigated the effect of surface modifications on flow boiling of water in a mini-channel of $25 \times 20 \times 0.4$ mm. The mini-channel was made of copper and three channels with different surface characteristics were investigated namely: sand blasted copper substrate, copper/diamond coating (diamond deposited on the copper surface) and diamond/carbon nano-tubes CNTs coating (diamond was deposited first on the copper surface then the CNTs were deposited over the diamond layer). The three surfaces were characterized using SEM analysis without reporting on the surface roughness of each surface. The SEM images indicated that the surface of the sand blasted copper, before depositing diamond on it, was rough, the copper surface coated with diamond was smooth without any cracks and the CNTs coating over the copper-diamond surface indicated that the nano-tubes were aligned vertically. Their experimental conditions covered three mass flux values, 283, 348 and 427 kg/m^2 s at a fixed inlet temperature of 90 °C. The measured contact angle for water over the three surfaces was 54.9° for the sand blasted surface, 89.9° for the copper-diamond coated surface and 133.5° for the CNT-coated surface. It was found that, for the three surfaces, nucleation (small bubbles) commenced in the downstream side of the channel, while CHF was triggered by severe vapour back flow. The nucleation density for the CNT-coated and diamond coated surfaces (non-wetting) was higher than that for the sand blasted surface. Flow visualization indicated that transition from bubbly to annular flow occurred rapidly, due to rapid bubble growth, for the sand blasted copper surface relative to the CNTs coated surface but slow compared to the diamond coated surface. The heat transfer measurements indicated that the CNT-coated surface performed better than the other two surfaces, particularly at the lowest mass flux. The critical heat flux of the CNT-coated surface was 22% higher at the lowest mass flux compared to the other tested surfaces. This percentage decreased to 6.7% at the highest mass flux. Also, the heat transfer coefficient increased by 31% at the lowest mass flux compared to the other

Please cite this article in press as: T.G. Karayiannis, M.M. Mahmoud, Flow boiling in microchannels: Fundamentals and applications, Appl. Therm. Eng. (2016), http://dx.doi.org/10.1016/j.applthermaleng.2016.08.063

examined surfaces. There was no significant difference in performance between the sand blasted and diamond-coated surfaces. This enhancement was attributed by Sunjith-Kumar et al. to the possibility that CNTs act as fins that increase the heat transfer surface area. The deterioration at high mass flux was attributed to the bending of the CNTs towards the surface, i.e. the nano tubes inclined to the surface rather than remaining normal to it.

It can be deduced from the above discussion that there is a small number of studies that investigated the effect of surface wettability on the local heat transfer coefficient for a wide range of experimental conditions. They were conducted at very low vapour quality and mass flux. Although they are not entirely conclusive, some concluding remarks can be summarized as follows: (1) Bubble size at boiling incipience for non-wetting surfaces is larger than that for wetting surfaces. This means that bubble flow diminishes for non-wetting surfaces and elongated bubble (slug) flow develops immediately at boiling incipience. (2) Boiling starts at a lower heat flux for non-wetting surfaces compared to the wetting surfaces. (3) Partial dryout occurs at higher vapour quality for the non-wetting surfaces. However, more experimental studies covering a wider range of experimental conditions are still required to reach rigid conclusions on the effect of surface wettability on flow boiling in microchannels.

8. Critical heat flux (CHF)

At the CHF conditions, the heat transfer rate deteriorates significantly and the surface temperature increases rapidly, which may result in burnout and failure of the device to be cooled. The change in surface temperature was the parameter mostly used by researchers to represent the occurrence of CHF. Thus, accurate prediction of flow boiling CHF is very important if reliable designs of microchannel heat sinks are to occur. CHF represents the upper thermal limit of the safe operation of any boiling device. Several researchers conducted parametric studies and proposed correlations for the prediction of CHF in small to micro diameter channels. These correlations are summarized in Table 2 and demonstrate that the most important parameters that were deemed to affect CHF are the fluid properties, the mass flux, the inlet sub-cooling and the channel length to diameter ratio. In order to have an insight into the effect of these parameters on CHF, all correlations were compared against each other using R-134a for a tube of 1 mm diameter with a 150 mm heated length. Fig. 18a depicts the effect of mass flux predicted by the various correlations at a fixed inlet sub-cooling of 2 K and 6 bar system pressure. It is obvious from the figure that all correlations agreed that the CHF increases as the mass flux increases, but the slope of the curve differs from one correlation to another, i.e. some correlations predict a moderate mass flux effect while others predict a strong mass flux effect. It is worth mentioning that some of the correlations summarized in Table 2, such as Qu and Mudawar [104] and Qi et al. [105], were not included in the figure because they predict values that are more than 10 times the values predicted by other correlations. Also, it is obvious from the figure that some correlations agree with each other, such as the Ong and Thome [106], Zhang et al. [107] and Mikielewicz et al. [108]. However, examining the results plotted indicates that there is no general agreement on the degree of dependence on the mass flux. In addition to that, all correlations summarized in Table 2 indicate no effect of the fluid inlet sub-cooling, except the correlations of Lazarek and Black [109] and Zhang et al. [107]. According to the correlation of Lazarek and Black [109], the CHF increases by 22% when the inlet sub-cooling increases from 1 to 30 K while the correlation of Zhang et al. predicts an opposite effect (21% reduction in CHF). The insignificant effect of inlet sub-cooling was reported by Qu and Mudawar [104] to be unique to multichannels compared to single channels. This was attributed to the observed instability prior to the critical heat flux in the multi-channels, such as flow reversal into the upstream plenum. This kind of instability has resulted in strong mixing between the vapour and the incoming fresh liquid and consequently the temperature of the fresh liquid increases and becomes close to saturation. However, some researchers, such as Wojtan et al. [102], investigated single channels and did not report an inlet sub-cooling effect.

Fig. 18b shows the effect of channel diameter on the CHF predicted by the various correlations for ΔT_{sub} = 2 K, P = 6 bar, G = 300 kg/m^2 s and 150 mm channel length. All correlations predicted that the CHF increases with increasing channel diameter except the correlation of Koşar et al. [6], which predicted a moderate decrease of CHF as the diameter increases. There is good

Table 2
Summary of flow boiling critical heat flux correlations proposed for micro scale application.

Author	Correlation	Remarks
Lazarek and Black [109]	$x_{crit} = 1 - 6.075 \times 10^{-3} GD^{0.25} \left(\frac{D}{L}\right)^{0.59} \left[1 + 3.11 \left(\frac{c_p \Delta T_{sub}}{h_{fg}}\right)\right]$	R-113, D = 3.1 mm, L = 123, 246 mm, G = 232–740 kg/m^2 s, P = 1.3–4.2 bar
Bowers and Mudawar [111]	$q''_{CHF} = 0.16 G h_{fg} We^{-0.19} (L/D)^{-0.54}$	R-113, D = 2.54, 0.51 mm, L = 10 mm, P = 1.38 bar, ΔT_{sub} = 10–32 K, G = 31–480 kg/m^2 s, no effect for ΔT_{sub}
Qu and Mudawar [104]	$\frac{q''_{CHF}}{G h_{fg}} = 33.43 \left(\frac{\rho_g}{\rho_L}\right)^{1.11} We_L^{-0.21} \left(\frac{L}{D}\right)^{-0.36}$	Water, R-113, D_h = 0.34 mm, G = 86–368 kg/m^2 s, ΔT_{sub} = 40, 70 K
Koşar et al. [6]	$q''_{CHF} = 0.0035 G h_{fg} We^{-0.12}$	Water, D_h = 0.227 mm, G = 41–302 kg/m^2 s
Kuan and Kandlikar [103]	$\frac{q''_{CHF}}{G h_{fg}} = 0.2305 \left(\frac{L}{D}\right)^{-0.9056}$	R-123, D = 0.27 mm
Wojtan et al. [102]	$q_{CHF} = 0.437 \left(\frac{\rho_g}{\rho_L}\right)^{0.073} We_L^{-0.24} \left(\frac{L}{D}\right)^{-0.72} G h_{fg}$	R-134a, R-245fa, D = 0.5, 0.8 mm
Zhang et al. [107]	$Bo = 0.0352 \left[We_D + 0.0119 (L/D_h)^{2.31} (\rho_g/\rho_L)^{0.361}\right]^{-0.295} \times (L/D_h)^{-0.311} \left[2.05 (\rho_g/\rho_L)^{0.17} - x_{in}\right]$	3837 data points, Water, D_h = 0.33–6.22 mm, P = 0.101–19 MPa, G = 5.33–1.34 × 10^5 kg/m^2 s, L/D = 1–975
Qi et al. [105]	$\frac{q_{CHF}}{G h_{fg}} = (0.214 + 0.14 Co) \left(\frac{\rho_g}{\rho_L}\right)^{0.133} We_L^{-1/3} \frac{1}{1 + 0.03 L/D}$	455 data points, Liquid nitrogen, D = 0.531, 0.834, 1.042, 1.931 mm, L = 250 mm
Agostini et al. [112]	$x_{crit} = \frac{q_{CHF}}{G(h_{fg} + h_{sub})} \frac{4L}{D}$	R-236fa, D_h = 0.336 mm
Ong and Thome [106]	$q_{CHF} = 0.12 G h_{fg} \left(\frac{\rho_g}{\rho_f}\right)^{0.062} We_L^{-0.141} \left(\frac{L}{D}\right)^{-0.7} \left(\frac{\mu_f}{\mu_g}\right)^{0.183} \left(\frac{D}{D_{th}}\right)^{0.11} D_{th} = 2\sqrt{\frac{\sigma}{g \Delta \rho}}$	Developed for single and multi-channels using R-134a, R-236fa and R245fa
Chen and Garimella [110]	$\frac{q''_{CHF}}{G h_{fg}} = 40 \left(\frac{\rho_g}{\rho_L}\right)^{1.12} We_d^{-0.24} \left(\frac{L}{D}\right)^{-0.34}$	
Mikielewicz et al. [108]	$\frac{q''_{CHF}}{G h_{fg}} = 0.62 \left(\frac{\rho_g}{\rho_L}\right)^{0.02} We_d^{-0.05} \left(\frac{L}{D}\right)^{-1.17}$	R-134a, R-123, SES36, ethanol, D = 1.15, 2.3 mm, L = 380 mm, x = 0.6–1, G = 40–900 kg/m^2 s, q = 20–220 kW/m^2

Please cite this article in press as: T.G. Karayiannis, M.M. Mahmoud, Flow boiling in microchannels: Fundamentals and applications, Appl. Therm. Eng. (2016), http://dx.doi.org/10.1016/j.applthermaleng.2016.08.063

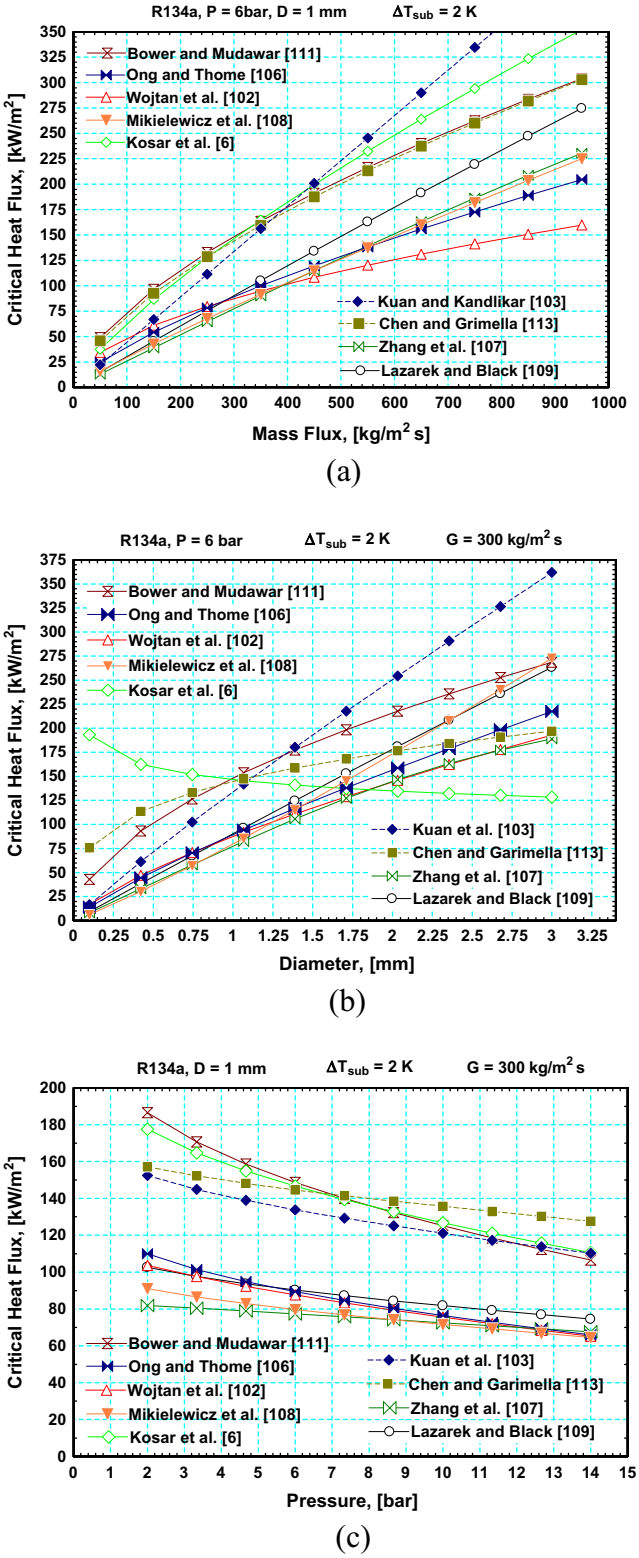

Fig. 18. Critical heat flux in flow boiling (a) effect of mass flux, (b) effect of diameter and (c) effect of pressure.

agreement between the correlations of Zhang et al. [107], Mikielewicz et al. [108], Wojtan et al. [102], Lazarek and Black [109], Ong and Thome [106] for D < 2 mm. However, the figure still shows large deviations between the correlations. Fig. 18c depicts the effect of system pressure on the CHF predicted by the correlations. The figure illustrates that all correlations agreed on the effect of system pressure on the CHF, where it decreases moderately as the system pressure increases. It is obvious also that the correlations of Kuan and Kandlikar [103], Chen and Garimella [110], Koşar et al. [6] and Bowers and Mudawar [111] predict values that are almost twice the values predicted by the other correlations. The effect of system pressure on the CHF arises from the effect of pressure on fluid properties. For R-134a, as the pressure increases from 6 to 14 bar, the gas density increases by 143%, the liquid density decreases by 10.6%, the gas to liquid-density ratio increases by 172%, the latent heat decreases by 18%, surface tension decreases by 46% and gas to liquid viscosity ratio increases by 67%. It can be concluded that CHF decreases as the gas to liquid density and viscosity ratio increases and as the latent heat and surface tension decreases.

This section demonstrates that there is a general consensus on the effect of different parameters on CHF. The deviations among all CHF correlations presented in this section could be due to the uncertainty in detecting the exact temperature excursion at the onset of CHF, which requires further investigation.

9. Design correlations

9.1. Prediction of flow patterns transitions

The prediction of the flow pattern transition boundaries is very important for the development of mechanistic heat transfer and pressure drop models. Chen [113] presented an empirical flow pattern transition model based on a large number of experimental data points (2392 data point) using R134a, D = 1.1–4.26 mm, P = 6–14 bar and G = 50–6400 kg/m^2 s. Karayiannis et al. [114] assessed this empirical map using experimental data of R245fa obtained using a 1.1 mm diameter tube and concluded that this map predicted all transition boundaries fairly well, except the bubbly to slug transition boundary. Mahmoud and Karayiannis [115] conducted an evaluation study of the existing micro scale flow patterns transition models and correlations using experimental data for R245fa. They found that there was a large discrepancy between all examined models and thus all models could not predict all the transition boundaries well, except the model given by Chen [113] that predicted all boundaries well, except the bubbly-slug transition boundary. Thus, they proposed a new criterion for the bubbly-slug transition boundary that was based on mechanistic assumptions, rather than on an empirical base. They summarized their prediction method, based on their and Chen [113] work, as follows:

Bubbly to slug transition: transition occurs when the Weber number, defined based on the relative velocity, equals a fixed value.

$$We_r = \frac{\rho_l U_r^2 D}{\sigma} = 4, \quad U_r = \frac{u_{gs}}{\alpha_c} - \frac{u_{ls}}{1-\alpha_c} \quad \alpha_c = 0.67 \tag{1}$$

Slug to churn transition: this boundary is described by three equations given below (2)–(4). The first equation predicts that the gas superficial velocity increases as the liquid superficial velocity increases in the low liquid velocity range. The second equation predicts that transition occurs at a fixed gas superficial velocity in the intermediate liquid velocity range. The third equation predicts that transition occurs at a lower gas superficial velocity as the liquid velocity increases in the high liquid velocity range.

$$u_h = 2.75\sqrt{\frac{\sigma}{f_l \rho_l D}} \tag{2}$$

$$u_{gs} = 587.1\left(\frac{\mu_l}{\rho_g D}\right)^{1.447}\left(\frac{\rho_g D}{\sigma}\right)^{0.937} \tag{3}$$

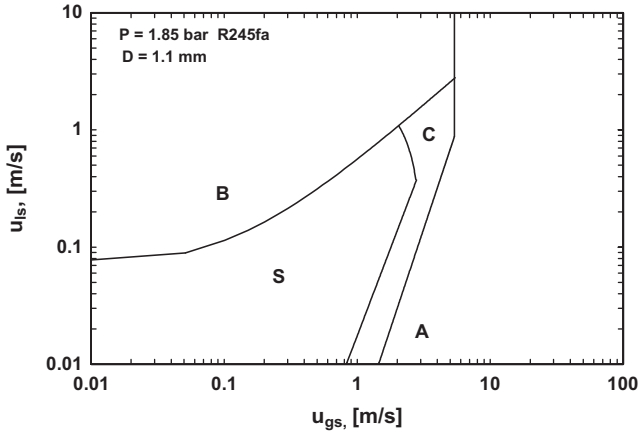

Fig. 19. The flow map proposed by Mahmoud and Karayiannis [115], B: bubbly, S: slug, C: churn, A: annular.

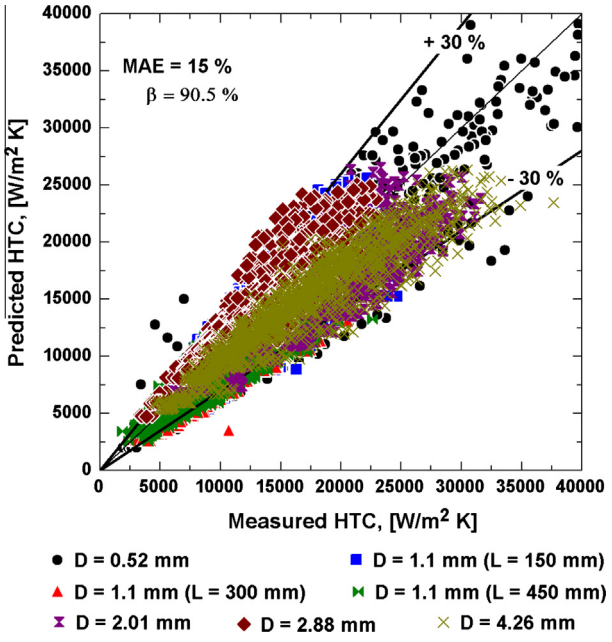

Fig. 20. Comparison of the Mahmoud and Karayiannis [117] correlation with the experimental database.

$$Re_{ls} = 81.08 We_{gs}^{1.626} Fr_{gs}^{*-0.267}, \quad Fr_{gs}^{*} = u_{gs}\sqrt{\rho_g/\Delta\rho g D} \tag{4}$$

Churn to annular: this boundary is described by the following two equations.

$$Fr_{gs}Re_{gs} = 3.119 \times 10^{5} \tag{5}$$

$$We_{ls} = 1.567 \times 10^{-17}(Fr_{gs}Re_{gs})^{3.41} \tag{6}$$

Fig. 19 below shows the proposed map for a diameter of 1.1 mm, R245fa and a system pressure of 1.85 bar.

9.2. Predictions of the heat transfer coefficient

Several correlations were proposed by different research groups for the prediction of the heat transfer coefficient in small to micro diameter channels. Mahmoud and Karayiannis [116] conducted an evaluation study for 21 macro and micro scale correlations and mechanistic models using experimental data for R-134a. The reader is referred to their paper for the summary and details of these models and correlations. They reported that all examined models and correlations failed to predict well their experimental data. Accordingly, the present authors proposed two different heat transfer correlations using a large experimental database that included 8561 data points for R134a with D = 4.26–0.52 mm. The details of these correlations can be found in Mahmoud and Karayiannis [116,117] and Mahmoud et al. [3]. The first correlation was based on fitting the experimental data as a function of dimensionless numbers, as given by the following equation:

$$\alpha_{tp} = \begin{cases} 3320 \dfrac{Bo^{0.63} We^{0.2} Re_f^{0.11}}{Co^{0.6}} \dfrac{k_f}{D} \\ \quad \text{for } D = 4.26, 2.88, 2.01, 1.1 \text{ before dryout and } 0.52 \text{ mm} \\ \quad \text{for } x < 0.3 \\ 5324 \left[\dfrac{Bo^{0.3} We^{0.25}}{N_{Co}^{0.25}}\right]^{1.79} \dfrac{k_f}{D} \\ \quad \text{for } D = 0.52 \text{ mm and } x > 0.3 \end{cases} \tag{7}$$

Fig. 20 depicts the performance of the Mahmoud and Karayiannis [116] correlation against the experimental data base. It shows that the correlation predicts 90.5% of the data to within ±30% with a 15% mean absolute error. This correlation was evaluated by Anwar et al. [118,119] who conducted flow boiling in vertical mini diameter tubes using R134a, R152a and R600a, see Fig. 21. Their

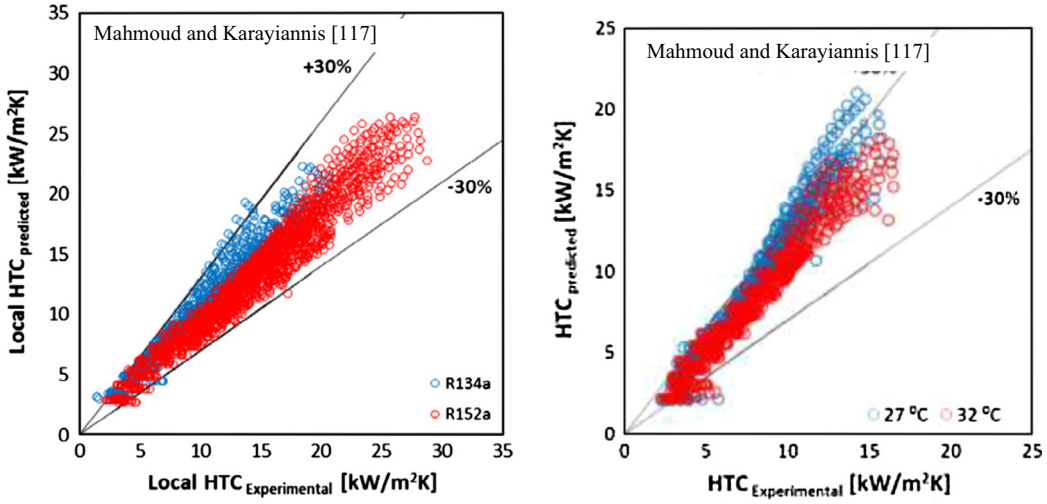

Fig. 21. Assessment of the Mahmoud and Karayiannis [117] correlation using R134a, R152a and R600a, Anwar et al. [118,119].

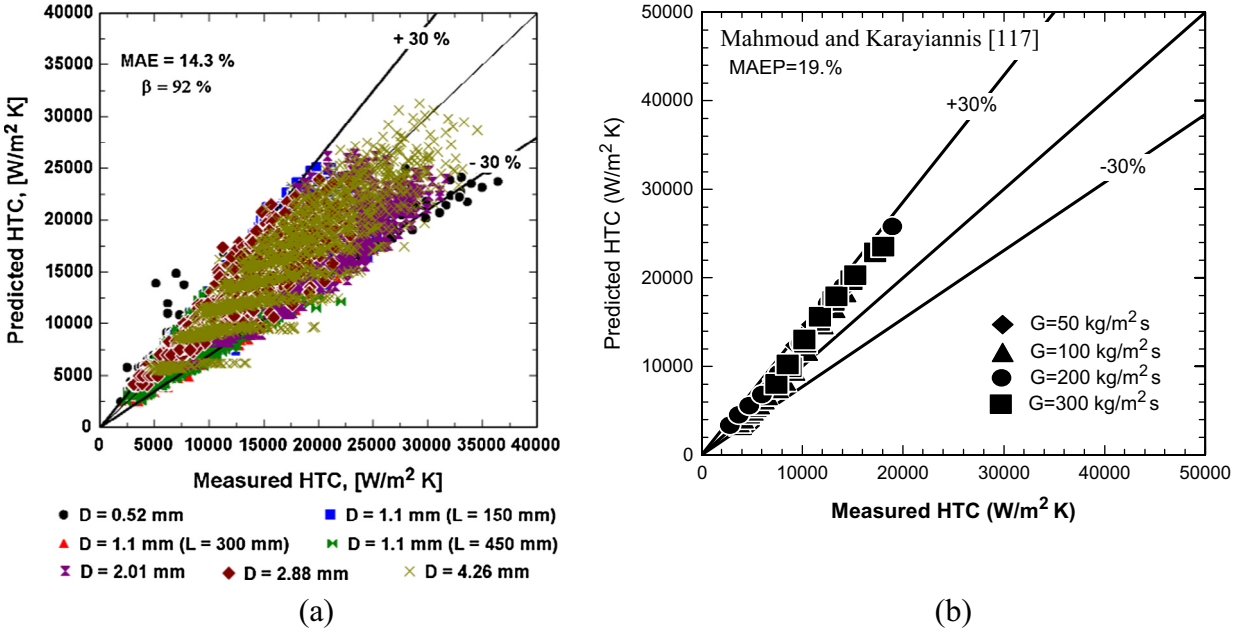

Fig. 22. The comparison of the Mahmoud and Karayiannis [116] Chen type correlation with (a) experimental data base and (b) experimental data of multi-microchannel evaporator using R134a, Fayyadh et al. [121].

comparison demonstrated that the correlation predicted 99.14% of the R152a data, 96.11% of the R134a data and 89.9% of the R600a data to within ±30%.

The second correlation was based on the model of Chen [120], which combined the contribution of nucleate and convective boiling mechanisms, as given by Eqs. (8)–(13).

$$\alpha_{tp} = S_{new}\alpha_{Cooper} + F_{new}\alpha_f \tag{8}$$

$$\alpha_f = \begin{cases} 4.36\frac{k_f}{D} & Re_f < 2000 \\ 0.023 Re_f^{0.8} \mathrm{Pr}_f^{0.4} \frac{k_f}{D} & Re_f > 3000 \end{cases} \tag{9}$$

$$Re_f = \frac{(1-x)GD}{\mu_f} \tag{10}$$

$$F_{New} = \left(1 + \frac{A}{X}\right)^{0.64} \tag{11}$$

$$A = 2.812 Co^{-0.408} \tag{12}$$

$$S_{New} = \frac{1}{1 + 2.56 \times 10^{-6}\left(Re_f F_{New}^{1.25}\right)^{1.17}} \tag{13}$$

Fig. 22a depicts the comparison of the Mahmoud and Karayiannis [116] correlation with the experimental data base and shows that 92% of the data were predicted to a MAE percentage of 14.3%. This correlation was assessed by Fayyadh et al. [121] using data for flow boiling of R134a in a multi-microchannel evaporator. The correlation predicted their data at a MAE of 19%, as seen in Fig. 22b.

10. Conclusions

The current paper presents an extensive review of current results and a discussion on flow boiling heat transfer in microchannels. The paper was divided into two parts. The first part discussed some possible applications for parallel, multi-microchannel heat sinks with an emphasis on the challenges in each application. The second part discussed the different fundamental issues of flow boiling in microchannels which are unresolved. The findings can be summarized as follows:

1. Flow boiling microchannel heat sinks are very promising for several applications, such as, the computer and IT industry, high power semiconductor devices, miniature vapour compression refrigeration systems and Proton Exchange Membrane Fuel cells. The average heat flux in computer chips is predicted to reach 2–4.5 MW/m^2, with local hot spots in the range 12–45 MW/m^2. In high power semi-conductor devices, such as IGBTs, the heat flux can be as high 6.3–50 MW/m^2 at the chip level.
2. There was very limited number of experimental studies on flow boiling in microchannels at operating conditions relevant to fuel cells applications, boiling in long or serpentine microchannels. Most research was directed towards boiling in short microchannels for cooling electronics components.
3. The design of future miniature cooling systems should take the issue of energy recovery into consideration, i.e. a significant amount of heat can be removed and reused in, for example, data centres.
4. There is no consensus on the criteria used for the definition of macro/small/mini/micro channels. The definition seems to be very complex for two phase flow, because all physics-based criteria were given as a function of fluid properties and flow parameters that depend on the actual operating conditions. The criteria used to identify flow patterns can result in different equations predicting the transition boundaries.
5. Although a significant amount of research studies were performed in small to micro diameter channels in the last two decades, there are no agreed conclusions on the dominant heat transfer mechanism(s). It seems that both nucleate and convective boiling mechanisms can contribute significantly and simultaneously to the heat transfer process in microchannels, and it is difficult to segregate the contribution of each mechanism.

Please cite this article in press as: T.G. Karayiannis, M.M. Mahmoud, Flow boiling in microchannels: Fundamentals and applications, Appl. Therm. Eng. (2016), http://dx.doi.org/10.1016/j.applthermaleng.2016.08.063

6. Flow reversal and instabilities were attributed by researchers to rapid bubble growth, the presence of a compressible volume ahead of the test section and nucleation near the channel inlet. The present authors suggest that channel surface characteristics, surface wettability, conjugate heat effects and the size of the inlet and outlet manifolds are important parameters that might affect flow instability and reversal. Additionally, there is a scarcity of experimental heat transfer data for stable and unstable boiling that would allow un understanding of the effect of flow reversal or oscillating flow on heat transfer. The oscillation of bubbles might enhance the heat transfer process in microchannels.
7. Channel surface characteristics have a significant effect on the behaviour of the local heat transfer coefficient at different heat and mass fluxes. This could result in different views on the dominant heat transfer mechanism(s) and thus may explain the discrepancy in the published heat transfer results and the mechanisms mentioned.
8. Few studies investigated the effect of surface wettability on flow boiling in microchannels and reported contradicting effects on boiling incipience.
9. There is a common agreement among researchers on the effect of mass flux, fluid properties, length to diameter ratio and inlet sub-cooling on flow boiling critical heat flux. However, there is a big deviation on the relative importance of each parameter with some researchers reporting a strong effect while some others reporting a weak effect. This deviation could be due to the difference in the criteria used to define the critical heat flux.
10. Design correlations for the prediction of flow patterns and heat transfer in small to micro diameter channels were developed, tested and are presented in the paper.

References

[1] S.-W. Kang, Y.T. Chen, G.-S. Chang, The manufacturing and test of (1 1 0) orientated silicon based micro heat exchanger, Tamkang J. Sci. Eng. 5 (3) (2002) 129–136.
[2] D.J. Chamund, L. Coulbeck, D.R. Newcombe, P.R. Waind, High power density IGBT module for high reliability applications, in: IEEE 6th Int. Power Electronics and Motion Control Conference, 17–20 May 2009, Wuhan, China, 2009.
[3] M.M. Mahmoud, T.G. Karayiannis, D.B.R. Kenning, in: Emerging Topics in Heat Transfer Enhancement and Heat Exchangers, WIT Press, 2014, pp. 321–396 (Chapter 10).
[4] A.G.A. Nnanna, W. Rutherford, W. Elomar, B. Sankowski, Assessment of thermoelectric module with nanofluid heat exchanger, Appl. Therm. Eng. 29 (2–3) (2009) 491–500.
[5] T.H. Yen, N. Kasagi, Y. Suzuki, Forced convective boiling heat transfer in microtubes at low mass and heat fluxes, Int. J. Multiphase Flow 29 (2003) 1771–1792.
[6] A. Koşar, C.-J. Kuo, Y. Peles, Boiling heat transfer in rectangular microchannels with reentrant cavities, Int. J. Heat Mass Transfer 48 (23–24) (2005) 4867–4886.
[7] I. Mudawar, Two phase microchannel heat sinks: theory, applications and limitations, J. Electron. Packag. 133 (2011) 041002:1–041002:31.
[8] C. Bachmann, A. Bar-Cohen, Hotspot remediation with anisotropic thermal interface materials, in: 11th IEEE Intersociety Conference on Thermal and Thermomechanical Phenomena in Electronic Systems, 28–31 May 2008, Orlando, FL, USA, 2008.
[9] B. Yang, P. Wang, A. Bar-Cohen, Mini-contact enhanced thermoelectric cooling of hot spots in high power devices, IEEE Trans. Compon. Packag. Technol. 30 (3) (2007) 432–438.
[10] J.F. Tullius, R. Vajtai, Y. Bayazitoglu, A review of cooling in microchannels, Heat Transfer Eng. 32 (7–8) (2011) 527–541.
[11] L. Jiang, J. Mikkelsen, J.-M. Koo, D. Huber, S. Yao, L. Zhang, P. Zhou, K.E. Goodson, Closed-loop electroosmotic microchannel cooling system for VLSI circuits, IEEE Trans. Compon. Packag. Technol. 25 (3) (2002) 347–355.
[12] J. Qu, H.-Y. Wu, Q. Wang, Experimental investigation of silicon-based micro-pulsating heat pipe for cooling electronics, Nanoscale Microscale Thermophys. Eng. 16 (2012) 37–49.
[13] Z. Wan, J. Deng, B. Li, X. Wang, Y. Xu, X. Wang, Y. Tang, Thermal performance of a miniature loop heat pipe using water-copper nanofluid, Appl. Therm. Eng. 78 (2015) 712–719.
[14] M. Fabbri, V.K. Dhir, Optimized heat transfer for high power electronic cooling using arrays of microjets, J. Heat Transfer 127 (7) (2005) 760–769.
[15] I. Mudawar, D. Bharathan, K. Kelly, S. Narumanchi, Two-phase spry cooling of hybrid vehicle electronics, IEEE Trans. Compon. Packag. Technol. 32 (2) (2009) 501–512.
[16] H. Bostanci, D.V. Ee, B.A. Saarloos, D.P. Rini, L.C. Chow, Spray cooling of power electronics using high temperature coolant and enhanced surface, in: 5th IEEE Vehicle Power and Propulsion Conference, 7–11 September 2009, Dearborn, MI 48128, 2009.
[17] Z. Zhao, Y. Peles, M.K. Jensen, Water jet impingement boiling from structures-porous surface, Int. J. Heat Mass Transfer 63 (2013) 445–453.
[18] E.A. Silk, E.L. Golliher, R. Paneer Selvam, Spray cooling heat transfer: technology overview and assessment of future challenges for micro-gravity application, Energy Convers. Manage. 49 (3) (2008) 453–468.
[19] D.B. Tuckerman, R.F.W. Pease, High performance heat sink for VLSI, IEEE Electron. Device Lett. 2 (1981) 126–129.
[20] W. Escher, T. Brunschwiler, B. Michel, D. Poulikakos, Experimental investigation of an ultrathin manifold microchannel heat sink for liquid-cooled chips, J. Heat Transfer 132 (8) (2010) 1–10.
[21] S.G. Kandlikar, T. Widger, A. Kalani, V. Mejia, Enhanced flow boiling over open microchannels with uniform and tapered gap manifolds, J. Heat Transfer 135 (6) (2013) 061401.
[22] L. Berkeley, R. Mahdavi, Liquid Cooling V. Air Cooling Evaluation in the Maui High Performance Computing Centre, Federal Energy Management Program, FEMP, 2014.
[23] J.B. Marcinichen, J.A. Olivier, N. Lamaison, J.R. Thome, Advances in electronics cooling, Heat Transfer Eng. 34 (5–6) (2013) 434–446.
[24] J. Pettersen, A. Hafner, G. Skaugen, H. Rekstad, Development of compact heat exchangers for CO_2 air conditioning systems, Int. J. Refrig. 21 (3) (1998) 180–193.
[25] P. Hrnjak, A.D. Litch, Microchannel heat exchangers for charge minimization in air-cooled ammonia condensers and chillers, Int. J. Refrig. 31 (4) (2008) 658–668.
[26] R. Mongia, K. Masahiro, E. Distefano, Small scale refrigeration system for electronics cooling within a notebook computer, in: The IEEE 10th Intersociety Conference on Thermal and Thermochemical Phenomena in Electronics Systems, 2006.
[27] Y.-T. Wu, C.-F. Ma, X.-H. Zhong, Development and experimental investigation of a miniature-scale refrigeration system, Energy Convers. Manage. 51 (1) (2010) 81–88.
[28] Z. Wu, R. Du, Design and experimental study of a miniature vapor compression refrigeration system for electronics cooling, Appl. Therm. Eng. 31 (2–3) (2011) 385–390.
[29] L.-Y. Jeng, T.-P. Teng, Performance evaluation of a hybrid cooling system for electronic chips, Exp. Therm. Fluid Sci. 45 (2013) 155–162.
[30] W. Yuan, B. Yang, Y. Yang, K. Ren, J. Xu, Y. Liao, Development and experimental study of the characteristics of a prototype miniature vapor compression refrigerator, Appl. Energy 143 (2015) 47–57.
[31] S. Truttasanawin, E.A. Groll, S.V. Garimella, Cremaschi, Experimental investigation of a miniature-scale refrigeration system for electronics cooling, IEEE Trans. Compon. Packag. Technol. 29 (3) (2006).
[32] A. Wintrich, U. Nicolai, W. Tursky, T. Reimann, Application Manual Power Semiconductors, ISLE Verlag, SEMIKRON International, 2011.
[33] D.L. Saums, Vaporizable dielectric fluid cooling of IGBT power semiconductors, in: Proc. Int. Symposium on Microelectronics, IMAPS 2009, 2009, pp. 238–249.
[34] F. Gao, B. Blunier, A. Miraoui, Proton Exchange Membrane Fuel Cell Modelling, ISTE Ltd. and John Willey and Sons, Inc., 2012.
[35] S. Pandiyan, K. Jayakumar, N. Rajalakshmi, K.S. Dhathathreyan, Thermal and electrical energy management in a PEMFC stack – an analytical approach, Int. J. Heat Mass Transfer 51 (3–4) (2008) 469–473.
[36] H. Pei, Z. Liu, H. Zhang, Y. Yu, Z. Tu, Z. Wan, W. Liu, In situ measurement of temperature distribution in proton exchange membrane fuel cell I a hydrogen-air stack, J. Power Sources 227 (2013) 72–79.
[37] F. Barreras, A. Lozano, J. Barroso, V. Roda, M. Maza, Theoretical model for the optimal design of air cooling systems of polymer electrolyte fuel cells: application to a high-temperature PEMFC, Fuel Cells 13 (2) (2013) 227–237.
[38] G. Zhang, S.G. Kandlikar, A critical review of cooling techniques in proton exchange membrane fuel cell stacks, Int. J. Hydrogen Energy 37 (3) (2012) 2412–2429.
[39] U. Soupremanien, S.L. Person, M. Favre-Marient, Y. Bultel, Tools for designing the cooling system of a proton exchange membrane fuel cell, Appl. Therm. Eng. 40 (2012) 161–173.
[40] R.K. Shah, D.P. Sekulić, Fundamentals of Heat Exchanger Design, John Willey and Sons, Inc., 2003.
[41] S.S. Mehendale, A.M. Jacobi, R.K. Shah, Fluid flow and heat transfer at micro- and meso-scales with application to heat exchanger design, Appl. Mech. Rev. 53 (7) (2000) 175–193.
[42] S.G. Kandlikar, W.J. Grande, Evolution of microchannel flow passages—thermohydraulic performance and fabrication technology, Heat Transfer Eng. 25 (1) (2003) 3–17.
[43] N. Brauner, D. Moalem-Maron, Identification of the range of small diameter conduits, regarding two-phase flow pattern transitions, Int. Commun. Heat Mass Transfer 19 (1992) 29–39.

Please cite this article in press as: T.G. Karayiannis, M.M. Mahmoud, Flow boiling in microchannels: Fundamentals and applications, Appl. Therm. Eng. (2016), http://dx.doi.org/10.1016/j.applthermaleng.2016.08.063

[44] P.A.K. Cornwell, P.A. Kew, Boiling in small parallel channels, in: P.A. Pilavachi (Ed.), Energy Efficiency in Process Technology, Elsevier Applied Science, London, 1993, pp. 624–638.
[45] M. Suo, P. Griffith, Two-phase flow in capillary tubes, J. Basic Eng. 86 (1964) 576–582.
[46] K.A. Triplett, S.M. Ghiaasiaan, S.I. Abdel-Khalik, D.L. Sadowski, Gas-liquid two-phase flow in microchannels, Part I: two-phase flow patterns, Int. J. Multiphase Flow 25 (1999) 377–394.
[47] A. Ullmann, N. Brauner, The prediction of flow pattern maps in minichannels, Multiphase Sci. Technol. 19 (1) (2007) 49–73.
[48] C.L. Ong, J.R. Thome, Macro-to-microchannel transition in two-phase flow: Part 1 – two phase flow patterns and film thickness measurements, Exp. Therm. Fluid Sci. 35 (2011) 37–47.
[49] T. Harirchian, S.V. Garimella, A comprehensive flow regime map for microchannel flow boiling with quantitative transition criteria, Int. J. Heat Mass Transfer 53 (2010) 2694–2702.
[50] C.B. Tibirica, G. Ribatski, Flow boiling phenomenological differences between micro-and macroscale channels, Heat Transfer Eng. 36 (11) (2015) 937–942.
[51] L. Chen, Y.S. Tian, T.G. Karayiannis, The effect of tube diameter on vertical two-phase flow regimes in small tubes, Int. J. Heat Mass Transfer 49 (2006) 4220–4230.
[52] P.M.-Y. Chung, M. Kawaji, The effect of channel diameter on adiabatic two-phase flow characteristics in microchannels, Int. J. Multiphase Flow 30 (2004) 735–761.
[53] Z.Y. Bao, D.F. Fletcher, B.S. Haynes, Flow boiling heat transfer of freon R11 and HCFC123 in narrow passages, Int. J. Heat Mass Transfer 43 (2000) 3347–3358.
[54] Z. Anwar, B. Palm, R. Khodabandeh, Flow boiling heat transfer and dryout characteristics of R152a in a vertical mini-channel, Exp. Therm. Fluid Sci. 53 (2014) 207–217.
[55] M.M. Mahmoud, D.B.R. Kenning, T.G. Karayiannis, Single and two phase heat transfer and pressure drop in a 0.52 mm vertical metallic tube, in: 7th Int. Conference on Enhanced, Compact and Ultra-Compact Heat Exchangers: From Microscale Phenomena to Industrial Applications, Heredia, Costa Rica, 13–18 September, 2009.
[56] S. Lin, P.A. Kew, K. Cornwell, Flow boiling of refrigerant R141b in small tubes, Trans. Inst. Chem. Eng. 79 (A) (2001) 417–424.
[57] D.A. McNeil, A.H. Raeisi, P.A. Kew, R.S. Hamed, Flow boiling heat-transfer in micro to macro transition flows, Int. J. Heat Mass Transfer 65 (2013) 289–307.
[58] W. Qu, I. Mudawar, Flow boiling heat transfer in two phase microchannel heat sinks: I. Experimental investigation and assessment of correlation methods, J Heat Mass Transfer 46 (2003) 2755–2771.
[59] H. Boye, Y. Staate, J. Schmidt, Experimental investigation and modelling of heat transfer during convective boiling in a minichannel, Int. J. Heat Mass Transfer 50 (2007) 208–215.
[60] S. Mortada, A. Zoughaib, C. Arzano-Daurelle, D. Clodic, Boiling heat transfer and pressure drop of R134a and R-1234yf in minichannels for low mass fluxes, Int. J. Refrig. 35 (2012) 962–973.
[61] C. Huh, M.H. Kim, An experimental investigation of flow boiling in an asymmetrically heated rectangular microchannel, Exp. Therm. Fluid Sci. 30 (2006) 775–784.
[62] S. In, S. Jeong, Flow boiling heat transfer characteristics of R123 and R134a in a micro-channel, Int. J. Multiphase Flow 35 (2009) 987–1000.
[63] R. Ali, B. Palm, M.H. Maqbool, Flow boiling heat transfer of refrigerants R134a and R245fa in a horizontal micro-channel, Exp. Heat Transfer 25 (2012) 181–196.
[64] K. Balasubramanian, M. Jagirdar, P.S. Lee, C.J. Teo, S.K. Chou, Experimental investigation of flow boiling heat transfer and instabilities in straight microchannels, Int. J. Heat Mass Transfer 66 (2013) 655–671.
[65] S. Basu, S. Ndao, G.J. Michna, Y. Peles, M.K. Jensen, Flow boiling of R134a in circular microtubes-Part I: study of heat transfer characteristics, J. Heat Transfer 133 (2011) 051502-1–051502-9.
[66] J.R. Thome, L. Consolini, Mechanisms of boiling in micro-channels: critical assessment, Heat Transfer Eng. 31 (4) (2010) 288–297.
[67] T. Harirchian, S.V. Garimella, Microchannel size effects on local flow boiling heat transfer to a dielectric fluid, Int. J. Heat Mass Transfer 51 (2008) 3724–3735.
[68] T. Harirchian, S.V. Garimella, Effects of channel dimension, heat flux, and mass flux on flow boiling regimes in microchannels, Int. J. Multiphase Flow 35 (2009) 349–362.
[69] N. Borhani, J.R. Thome, Intermittent dewetting and dryout of annular flows, Int. J. Multiphase Flow 67 (s) (2014) 144–152.
[70] S.G. Kandlikar, P. Balasubramanian, An experimental study on the effect of gravitational orientation on flow boiling of water in 1054 × 197 μm parallel minichannels, J. Heat Transfer 127 (2005) 820–829.
[71] J.R. Thome, V. Dupont, A.M. Jacobi, Heat transfer model for evaporation in microchannels, Part I: presentation of the model, Int. J. Heat Mass Transfer 47 (2004) 3375–3385.
[72] S. Bigham, S. Moghaddam, Microscale study of mechanisms of heat transfer during flow boiling in a microchannel, Int. J. Heat Mass Transfer 88 (2015) 111–121.
[73] G. Wang, P. Cheng, H. Wu, Unstable and stable flow boiling in parallel microchannels and in a single microchannel, Int. J. Heat Mass Transfer 50 (21–22) (2007) 4297–4310.
[74] X. Fu, S.L. Qi, P. Zhang, R.Z. Wang, Visualization of flow boiling of liquid nitrogen in a vertical mini-tube, Int. J. Multiphase Flow 34 (4) (2008) 333–351.
[75] M.R. Aligoodarz, Y. Yan, D.B.R. Kenning, Wall temperature and pressure variations during flow boiling in narrow channels, Proc.11th Int. Heat Transfer Conference (IHTC), August 23–28, vol. 2, 1998, pp. 225–230.
[76] S.L. Qi, P. Zhang, R.Z. Wang, L.X. Xu, Flow boiling of liquid nitrogen in micro-tubes: Part I – the onset of nucleate boiling, two-phase flow instability and two-phase flow pressure drop, Int. J. Heat Mass Transfer 50 (25–26) (2007) 4999–5016.
[77] D. Bogojevic, K. Sefiane, A.J. Walton, H. Lin, G. Cummins, Two-phase flow instabilities in a silicon microchannels heat sink, Int. J. Heat Fluid Flow 30 (2009) 854–867.
[78] W. Wang, K. Sefiane, Z.-G. Wang, S. Harmand, Analysis of two phase pressure drop fluctuations during microchannel flow boiling, Int. J. Heat Mass Transfer 70 (2014) 353–362.
[79] M.R. Özdemir, M.M. Mahmoud, T.G. Karayiannis, Flow boiling heat transfer in a rectangular copper microchannel, Int. Conference on Advances in Mechanical Engineering, 13–15 May, Yildiz Technical University, Istanbul, Turkey, 2015.
[80] Y. Yan, D.B.R. Kenning, Pressure and temperature fluctuations during boiling in narrow channel, in: Heat Transfer in Condensation and Evaporation, Grenoble, Eurotherm 62 (1998) 107–1223.
[81] S. Gedupudi, Y.Q. Zu, T.G. Karayiannis, D.B.R. Kenning, Y.Y. Yan, Confined bubble growth during flow boiling in a mini/micro-channel of rectangular cross-section Part I: experiments and 1-D modelling, Int. J. Therm. Sci. 50 (2011) 250–266.
[82] S. Gedupudi, D.B.R Kenning, T.G Karayiannis, Flow boiling in rectangular microchannels: 1-D modelling of the influence of inlet resistance on flow reversal, in: 4th Micro and Nano Flows Conference, UCL, London, UK, 7–10 September, 2014.
[83] Y. Liu, D.F. Fletcher, B.S. Haynes, On the importance of upstream compressibility in microchannel boiling heat transfer, Int. J. Heat Mass Transfer 58 (2013) 503–512.
[84] S.G. Kandlikar, Nucleation characteristics and stability considerations during flow boiling in microchannels, Exp. Therm. Fluid Sci. 30 (2006) 441–447.
[85] E.M. Fayyadh, M.M. Mahmoud, T.G. Karayiannis, Flow boiling heat transfer of R134a in multi microchannels, Int. J. Heat Mass Transfer (2016) (Submitted for publication).
[86] A. Koşar, C.-J. Kuo, Y. Peles, Suppression of boiling flow oscillations in parallel microchannels by inlet restrictors, J. Heat Transfer 128 (3) (2006) 251–260.
[87] W.K. Kuan, S.G. Kandlikar, Experimental study on the effect of stabilization on flow boiling heat transfer in microchannels, Heat Transfer Eng. 28 (8–9) (2007) 746–752.
[88] C.T. Lu, C. Pan, Stabilization of flow boiling in microchannel heat sinks with a diverging cross-section design, J. Micromech. Microeng. 18 (7) (2008) 075035.
[89] A. Tamanna, P.S. Lee, Flow boiling instability characteristics in expanding silicon microgap heat sink, Int. J. Heat Mass Transfer 89 (2015) 390–405.
[90] L. King, S.S. Sadhal, Effect of surfactants on the growth and departure of bubbles from solid surfaces, Heat Mass Transfer 50 (2014) 373–382.
[91] J.G. Collier, J.R. Thome, Convective Boiling and Condensation, third ed., Oxford University Press, Oxford, UK, 1994.
[92] M.M. Mahmoud, T.G. Karayiannis, D.B.R. Kenning, Surface effects in flow boiling of R134a in microtubes, Int. J. Heat Mass Transfer 45 (15–16) (2011) 3334–3346.
[93] T.G. Karayiannis, M.M. Mahmoud, D.B.R. Kenning, A study of discrepancies in flow boiling results in small to microdiameter metallic tubes, Exp. Therm. Fluid Sci. 36 (2012) 126–142.
[94] B.J. Jones, S.V. Garimella, Surface roughness effects on flow boiling in microchannels, J. Therm. Sci. Eng. Appl. 1 (2009) 041007-1.
[95] T. Alam, P.S. Lee, C.R. Yap, Effect of surface roughness on flow boiling in silicon microgap heat sinks, Int. J. Heat Mass Transfer 64 (2013) 28–41.
[96] E.A. Pike-Wilson, T.G. Karayiannis, Flow boiling of R245fa in 1.1 mm diameter stainless steel, brass and copper tube, Exp. Therm. Fluid Sci. 59 (2014) 166–183.
[97] T. Cikim, E. Armagan, G.O. Ince, A. Kosar, Flow boiling enhancement in microtubes with crosslinked pHEMA coatings and the effect of coating thickness, J. Heat Transfer 136 (2014) 081504-1.
[98] T.Y. Liu, P.L. Li, C.W. Liy, C. Gau, Boiling flow characteristics in microchannels with very hydrophobic surface to super-hydrophilic surface, Int. J. Heat Mass Transfer 54 (2011) 126–134.
[99] C. Choi, J.S. Shin, D.I. Yu, M.H. Kim, Flow boiling behaviours in hydrophilic and hydrophobic microchannels, Exp. Therm. Fluid Sci. 35 (2011) 816–824.
[100] H.T. Phan, N. Caney, P. Marty, S. Colasson, J. Gavillet, Flow boiling of water on nanocoated surfaces in a microchannel, J. Heat Transfer 134 (2012) 020901-1.
[101] C.S. Sujith, S. Suresh, L. Yang, Q. Yang, S. Aravind, Flow boiling heat transfer enhancement using carbon nanotube coating, Appl. Therm. Eng. 65 (2014) 166–175.
[102] L. Wojtan, R. Revellin, J.R. Thome, Investigation of saturated critical heat flux in a single, uniformly heated microchannel, Exp. Therm. Fluid Sci. 30 (8) (2006) 765–774.
[103] W.K. Kuan, S.G. Kandlikar, Critical heat flux measurement and model for refrigerant-123 under stabilized flow conditions in microchannels, ASME Proc. Heat Transfer (2006) 285–295 (Paper No. IMECE2006-13310).
[104] W. Qu, I. Mudawar, Measurement and correlation of critical heat flux in two phase microchannel heat sinks, Int. J. Heat Mass Transfer 47 (2004) 2045–2059.

Please cite this article in press as: T.G. Karayiannis, M.M. Mahmoud, Flow boiling in microchannels: Fundamentals and applications, Appl. Therm. Eng. (2016), http://dx.doi.org/10.1016/j.applthermaleng.2016.08.063

[105] S.L. Qi, P. Zhang, R.Z. Wang, L.X. Xu, Flow boiling of liquid nitrogen in micro-tubes: Part II – heat transfer characteristics and critical heat flux, Int. J. Heat Mass Transfer 50 (25–26) (2007) 5017–5030.
[106] C.L. Ong, J.R. Thome, Macro-to-microchannel transition in two-phase flow: Part II – flow boiling heat transfer and critical heat flux, Exp. Therm. Fluid Sci. 35 (6) (2011) 873–886.
[107] W. Zhang, T. Hibiki, K. Mishima, Y. Mi, Correlation of critical heat flux for flow boiling of water in minichannels, Int. J. Heat Mass Transfer 49 (5–6) (2006) 1058–1072.
[108] D. Mikielewicz, J. Wajs, M. Glinski, A.-B.R.S. Zrooga, Experimental investigation of dryout of SES 36, R134a, R123 and ethanol in vertical small diameter tubes, Exp. Therm. Fluid Sci. 44 (2013) 556–564.
[109] G.M. Lazarek, S.H. Black, Evaporative heat transfer, pressure drop and critical heat flux in a small vertical tube with R-113, Int. J. Heat Mass Transfer 25 (7) (1982) 945–960.
[110] T. Chen, S.V. Garimella, A study of critical heat flux during flow boiling in microchannel heat sinks, J. Heat Transfer 134 (2012) 011504-1.
[111] M.B. Bowers, I. Mudawar, High flux boiling in low flow rate, low pressure drop minichannel and microchannel heat sinks, Int. J. Heat Mass Transfer 37 (2) (1994) 321–332.
[112] B. Agostini, R. Revellin, J.R. Thome, M. Fabbri, B. Michel, D. Calmi, U. Kloter, High heat flux flow boiling in silicon multi-microchannels – Part III: saturated critical heat flux of R236fa and two-phase pressure drops, Int. J. Heat Mass Transf. 51 (21–22) (2008) 5426–5442.
[113] L. Chen, Flow Patterns in Upward Two-phase Flow in Small Diameter Tubes PhD Thesis, Brunel University London, UK, 2006.
[114] T.G. Karayiannis, E.A. Pike-Wilson, L. Chen, M. Mahmoud, Y. Tian, Flow patterns and comparison with correlations for vertical flow boiling of R245fa in small to micro tubes, in: 4th Micro and Nano Flows Conference UCL, London, UK, 7–10 September, 2014.
[115] M.M. Mahmoud, T.G. Karayiannis, Flow pattern transition models and correlations for flow boiling in mini-tubes, J. Exp. Therm. Fluid Sci. 70 (2016) 270–282.
[116] M.M. Mahmoud, T.G. Karayiannis, Heat transfer correlation for flow boiling in small to micro tubes, Int. J. Heat Mass Transfer 66 (2013) 553–574.
[117] M. Mahmoud, T. Karayiannis, A statistical correlation for flow boiling heat transfer in micro tubes, in: Proceedings of the 3rd European Conference on Microfluidics – Microfluidics 2012, Heidelberg, Germany, December 3–5, 2012.
[118] Z. Anwar, B. Palm, R. Khodabandeh, Flow boiling of R600a in a uniformly heated vertical minichannel, in: Proc. 13th UK Heat Transfer Conference, Imperial College London, 2013.
[119] Z. Anwar, B. Palm, R. Khodabandeh, Flow boiling heat transfer and dryout characteristics of R152a in a vertical mini-channel, Exp. Therm. Fluid Sci. 53 (2014) 207–217.
[120] J.C. Chen, A correlation for boiling heat transfer to saturated fluids in convective flow, Ind. Eng. Chem. 5 (1966) 322–329.
[121] E.M. Fayyadh, M.M. Mahmoud, T.G. Karayiannis, Flow boiling heat transfer of R134a in multi microchannels, in: Proceedings of the 2nd International Conference on Heat Transfer and Fluid Flow, Barcelona, Spain, July 20–21, 2015.

Please cite this article in press as: T.G. Karayiannis, M.M. Mahmoud, Flow boiling in microchannels: Fundamentals and applications, Appl. Therm. Eng. (2016), http://dx.doi.org/10.1016/j.applthermaleng.2016.08.063